HIGHER-ORDER PHASE FIELD MODELS FOR FRACTURE

ISAAC J. LEE, THOMAS J. R. HUGHES

Abstract. In the variational approach to fracture, we capture the behavior of cracks in a body by minimizing the body's potential energy [3]. However, the energy functional contains a surface integral over the unknown crack surface, and this makes the minimization difficult. To solve this issue, Bourdin, Francfort, and Marigo developed an approximation of the functional by replacing the surface integral with a volume integral [2]. The approximation also introduced the notion of using a phase field—a *continuous* function—to indicate whether the body is fractured at a given point.

In the isogeometric approach, we use smooth B-splines to represent the geometry of the body and the fields in question. This lets us accurately solve the governing PDEs. Recently, Borden extended Bourdin's second-order theory to a fourth-order theory, and obtained better results using quadratic B-splines as basis functions [1]. (The order of the theory refers to that of the differential equation involving the phase field.)

In this work, we go even further and develop the sixth- and the eighth-order theories. A sixth-order theory warrants our attention, in particular, as we can then use cubic B-splines, the standard in CAD industry.

Numerical results from a 1D problem show that we can get even better results using the sixth- and eighth-order theories, provided the minimization is done correctly. We find that, for all theories, constraints must be supplied for the phase field and must be satisfied in a numerical simulation (which we do so using augmented Lagrangian method). This means, we had approached the second- and fourth-order theories in an erroneous manner, and we must more carefully examine the past and the ongoing works that involve a phase field.

1. Summary of Second- and Fourth-Order Theories

In the variational approach to fracture, we minimize the body's potential energy to determine its state. Without loss of generality, we consider a quasi-static, brittle fracture, and neglect body force and surface tractions. Then, the potential energy Ψ is the sum of two terms—the elastic strain energy and a surface energy due to fracture:

$$\Psi = \Psi(\vec{u}, \Gamma_{\text{crack}}) \equiv \int_{\Omega \setminus \Gamma_{\text{crack}}} \psi_e(\vec{u})\, dx + \int_{\Gamma_{\text{crack}}} G_c\, ds. \tag{1.1}$$

We will use the following notations throughout this paper:

Ω	the body in consideration
Γ_{crack}	the fracture surface
x	a point in the body
dx, ds	volume and surface differentials
ψ_e	elastic strain energy (per unit volume)
$\vec{u}$	displacement of the body
G_c	critical fracture energy (per unit area, constant).

As the cracks are to evolve over time (Γ_{crack} changes), the minimization of Ψ is rather difficult—both analytically and numerically.

To solve this issue, we introduce a continuous function $c = c(x) \in [0, 1]$ to indicate whether the body is fractured at a given point x. We call the function c the **phase field**. We let $c(x) = 0$ if the body is fractured at x, and $c(x) = 1$ if the body is intact at x. How fast c transitions between 0 and 1 can be controlled by a parameter $\ell_0 > 0$.

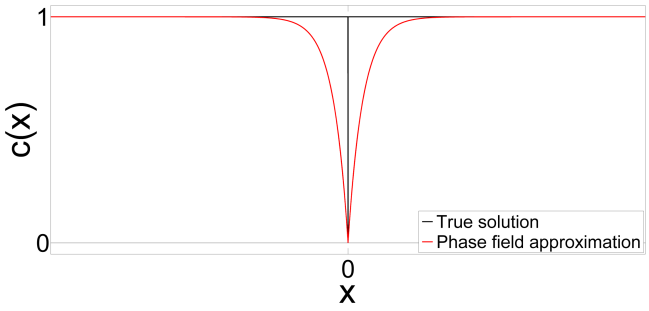

Figure 1.1. We use a continuous function to show where the body is fractured.

Next, we assume that the strain energy over the intact domain $\Omega \setminus \Gamma_{\text{crack}}$ is equivalent to that over the entire domain Ω, if we can properly "degrade" the strain energy in the damaged region using the phase field. So we make the following approximation:

$$\int_{\Omega} c^2\, \psi_e(\vec{u})\, dx \;\approx\; \int_{\Omega \setminus \Gamma_{\text{crack}}} \psi_e(\vec{u})\, dx. \tag{1.2}$$

We see that the relation above is an equality if there is no damage anywhere.

Finally, we assume that there is an expression Γ_c that involves the phase field c and the parameter ℓ_0, such that we can approximate the surface integral in Ψ with a volume integral over the entire body, i.e.

$$\int_\Omega G_c \, \Gamma_c \, dx \approx \int_{\Gamma_{\text{crack}}} G_c \, ds. \tag{1.3}$$

To be precise, we will call Γ_c the **crack density**, and the volume integral in (1.3) the **crack density functional**.

Then, we can instead minimize the approximate energy $\Psi = \Psi(\vec{u}, c)$, where

$$\boxed{\Psi(\vec{u}, c) = \int_\Omega c^2 \, \psi_e(\vec{u}) \, dx + \int_\Omega G_c \, \Gamma_c \, dx}. \tag{1.4}$$

This method has the advantage that a crack's behavior is determined solely by the PDEs that come from (1.4). No ad-hoc rules are needed to decide propagation, nucleation, or bifurcation of the crack. Of course, we must carefully consider how the minimizers $(\vec{u}, c)$ behave as we let $\ell_0 \to 0^+$. In particular, do the minimizers of the approximate energy converge to that of the original, and in what sense? This brings the notion of Gamma convergence, which is not easy to prove.

1.1. Second-Order Theory

Throughout the paper, we will consider the 1D problem of an elastic bar in tension to motivate the expression for Γ_c. The bar is infinite in length, and has a crack "in the middle" at $x = 0$. The phase field, had we allowed it to be discontinuous, would be equal to 1 everywhere except $x = 0$, where it would be equal to 0. (The bar has Young's modulus E, and a constant critical fracture energy G_c.)

We prescribe Dirichlet BCs to the displacement field by fixing the "left end" of the bar and pulling the "right end" by some amount, $u_0 \, (> 0)$. This will generate a displacement field that is piecewise constant: $u(x) = 0$ if $x < 0$, and $u(x) = u_0$ if $x > 0$.

As a result, the strain energy in (1.4) is equal to zero (provided that we have $c(0) = 0$ so that the integral makes sense), and the potential energy is minimized when the surface energy is minimized. There is a caveat, however: $c(0) = 0$ acts a continuity condition for the phase field, so the domain of the body is $\Omega = \mathbb{R} \setminus \{0\}$, not $\Omega = \mathbb{R}$.

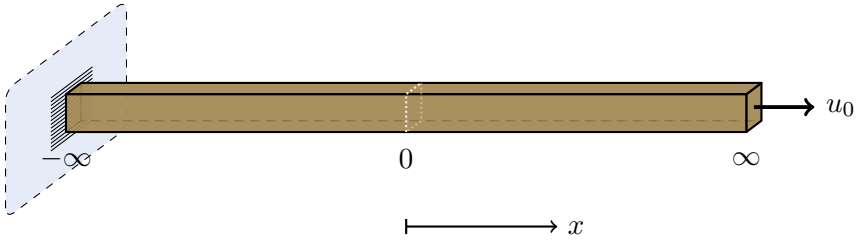

FIGURE 1.2. Schematics for the 1D problem of a bar in tension.

However, the phase field must be continuous. So let us approximate the discontinuous function with a C^0-function (see Figure 1.1):

$$\boxed{c(x) = 1 - \exp\Big(-\frac{1}{2}\frac{|x|}{\ell_0}\Big)}. \tag{1.5}$$

We can show that this c uniquely satisfies the following differential equation and the continuity and remote conditions:

$$\begin{cases} c - 4\ell_0^2\, c'' = 1, \ \text{ for } x \in \Omega \\ c(0) = 0 \\ c(x) \to 1, \ \text{ as } |x| \to \infty. \end{cases}$$

Now, if this equation were an Euler-Lagrange (EL) equation, then by construction, the function c would be a critical point. It so happens that we can "invert" this equation to get a crack density functional. We will denote the crack density by $\Gamma_{c,2}$:

$$\boxed{\Gamma_{c,2} = \frac{1}{4\ell_0}\Big[(1-c)^2 + 4\ell_0^2\,(c')^2\Big]}, \tag{1.6}$$

In summary, c minimizes the functional $\int \Gamma_{c,2}\ dx$ subject to the two conditions above. It gives us the (global) minimum, as $\Gamma_{c,2}$ is convex over the admissible functions c. Furthermore, with the minimizer c, we get

$$\int_\Omega \Gamma_{c,2}\ dx = 1,$$

i.e. the volume integral matches the surface integral exactly (in 1D).

In the general three-dimensional setting, we let the crack density be

$$\Gamma_{c,2} = \frac{1}{4\ell_0}\Big[(1-c)^2 + 4\ell_0^2\,|\nabla c|^2\Big],$$

and would have the Laplacian operator Δ for the second derivative in the EL equation. We refer to this as the **second-order theory**, because the EL equation is second-order.

1.2. Fourth-Order Theory

This time, we approximate the discontinuous function with a C^1-function,

$$\boxed{c(x) = 1 - \exp\Big(-\frac{|x|}{\ell_0}\Big)\Big[1 + \frac{|x|}{\ell_0}\Big]}, \tag{1.7}$$

which satisfies the following equation and the continuity and remote conditions:

$$\begin{cases} c - 2\ell_0^2\, c'' + \ell_0^4\, c^{(4)} = 1, \ \text{ for } x \in \Omega \\ c(0),\, c'(0) = 0 \\ c(x) \to 1, \ c'(x) \to 0, \ \text{ as } |x| \to \infty. \end{cases}$$

We can "invert" the equation above to obtain a crack density functional. The crack density is denoted by $\Gamma_{c,4}$:

$$\boxed{\Gamma_{c,4} = \frac{1}{4\ell_0}\Big[(1-c)^2 + 2\ell_0^2\,(c')^2 + \ell_0^4\,(c'')^2\Big]}. \tag{1.8}$$

By construction, c is the global minimizer to $\int \Gamma_{c,4}\,dx$, subject to the four constraints. Furthermore, with this c,

$$\int_\Omega \Gamma_{c,4}\,dx = 1,$$

i.e. the volume integral matches the surface integral exactly (in 1D).

In the general three-dimensional setting, we let

$$\Gamma_{c,4} = \frac{1}{4\ell_0}\Big[(1-c)^2 + 2\ell_0^2\,|\nabla c|^2 + \ell_0^4\,(\Delta c)^2\Big],$$

and would have the biharmonic operator Δ^2 for the fourth derivative in the EL equation. We refer to this as the **fourth-order theory**.

1.3. Remarks

In retrospect, we examined a sharp interface problem, where a crack is represented by a discontinuous field. We came up with a continuous function to approximate it, and called this the phase field.

By examining the derivatives of the phase field, we wrote an equation that it satisfies, and the equation happened to be an EL equation for a crack density functional. Note that the phase field can minimize any positive multiple of the crack density functional. The crack densities (1.6) and (1.8) had been scaled appropriately (normalized) so that the volume integral would match the surface integral when it is minimized in 1D.

With this constructive approach, we have the analytical solution for the phase field. Hence, we know what the finite element solution should look like and converge to. Had we instead started by guessing a crack density functional, e.g. based on existing literature, we might not have been able to solve the EL equation to find the global minimizer, i.e. the analytical solution for the phase field. Without the global minimum value, normalization would not be possible either.

The crack densities $\Gamma_{c,2}$ and $\Gamma_{c,4}$ are functions of the phase field c (of course, ℓ_0 too). The notations $\Gamma_2(c)$ and $\Gamma_4(c)$ are perhaps more correct, but we will continue to use $\Gamma_{c,2}$ and $\Gamma_{c,4}$, since they look similar to the notation Γ_{crack} and measure the crack surface in some sense. The expressions of $\Gamma_{c,2}$ and $\Gamma_{c,4}$ are valid in the physical domain Ω, so quadrature must be done accordingly.

The variational approach to brittle fracture was conceived by Francfort and Marigo [3]. Prior to this, the Mumford-Shah functional was used for image segmentation. It contained a surface integral, which was approximated by a volume integral (the result is called the Ambrosio-Tortorelli functional). Bourdin and the two saw the connection to fracture and proposed the second-order theory, introducing the notion of a phase field for fracture in the process [2]. Later, Borden et al. extended the work by developing the fourth-order theory and examining ductile fracture [1].

1.4. Appendix for Section 1

We made two claims while demonstrating the second-order theory (and similarly, the fourth-order theory). First, that the phase field (1.5) uniquely solves the EL equation. Secondly, that this phase field gives us the minimum (instead of maximum). The proofs are simple, so we will include them here.

Suppose that $d = d(x)$ is another function that satisfies the equation and the BCs. The difference $e := c - d$ then satisfies the following homogeneous equation and BCs:

$$\begin{cases} e - 4\ell_0^2\, e'' = 0, \ \text{ for } x \in \Omega \\ e(0) = 0 \\ e(x) \to 0, \ \text{ as } |x| \to \infty. \end{cases}$$

From the homogeneous equation, we see that e takes the form,

$$e(x) = e_0 + e_1 \exp\Big(\frac{x}{2\ell_0}\Big) + e_2 \exp\Big(-\frac{x}{2\ell_0}\Big).$$

By the continuity condition and the remote conditions, we must have

$$e_0 = 0, \quad e_1 = 0, \quad e_2 = 0.$$

Hence, $c \equiv d$.

Now, let us show that $\int \Gamma_{c,2}\, dx$ is convex, i.e. that $\Gamma_{c,2}$ is convex over the admissible functions c. For clarity, here we denote the crack density by $\Gamma_2 = \Gamma_2(c)$.

Let c and d be admissible functions, and $t \in [0,\, 1]$. Then,

$$\begin{aligned} \Gamma_2(tc + (1-t)d) &= \frac{1}{4\ell_0}\Big[\big(1 - tc - (1-t)d\big)^2 + 4\ell_0^2\,\big(tc' + (1-t)d'\big)^2\Big] \\ &= \frac{1}{4\ell_0}\Big[\big(t(1-c) + (1-t)(1-d)\big)^2 + 4\ell_0^2\,\big(tc' + (1-t)d'\big)^2\Big] \\ &\le \frac{1}{4\ell_0}\Big[\big(t(1-c)^2 + (1-t)(1-d)^2\big) + 4\ell_0^2\,\big(t(c')^2 + (1-t)(d')^2\big)\Big] \\ &= t\,\Gamma_2(c) + (1-t)\,\Gamma_2(d). \end{aligned}$$

Since the phase field c uniquely satisfies the EL equation, the minimum is global.

2. Developing Higher-Order Theories

In the previous section, we argued that we can easily develop a phase field model of a given order if we follow this recipe consisting of three ingredients:

> ① Phase field
> Come up with a phase field that approximates the sharp interface limit and has a certain level of smoothness over the domain.
>
> ② Differential equation + BCs
> The equation, together with BCs, is an EL equation that the phase field uniquely satisfies.
>
> ③ Crack density
> The crack density functional leads to the EL equation and has been normalized.

Let us consider what happens if we replace the linear polynomial in the phase field from the fourth-order theory with a quadratic or a cubic polynomial. Recall that we are working with a bar of infinite length, with a crack at $x = 0$. The domain of the body is $\Omega = \mathbb{R} \setminus \{0\}$, due to the fact that we apply continuity conditions at the crack.

2.1. Sixth-Order Theory

Based on our knowledge about the second- and fourth-order theories, let us suppose that the phase field c and the crack density $\Gamma_{c,6}$ take the following forms:

$$\boxed{\begin{aligned} c(x) &= 1 - \exp\Big(-k\,\frac{|x|}{\ell_0}\Big)\Big[c_0 + c_1\,\frac{|x|}{\ell_0} + c_2\,\frac{|x|^2}{\ell_0^2}\Big], \\ \Gamma_{c,6} &= \frac{1}{4\ell_0}\Big[(1-c)^2 + a_1\,(c')^2 + a_2\,(c'')^2 + a_3\,(c''')^2\Big]. \end{aligned}} \tag{2.1}$$

Here, $k > 0$, $\{c_0,\, c_1,\, c_2\}$, $\{a_1,\, a_2,\, a_3\}$ are constants to be found.

Assume that the phase field c solves the minimization problem,

$$\text{minimize} \quad \int_\Omega \Gamma_{c,6}\; dx$$

$$\text{subject to} \quad \begin{cases} c(0),\, c'(0),\, c''(0) = 0 \\ c(x) \to 1,\;\; c'(x),\, c''(x) \to 0, \quad \text{as } |x| \to \infty. \end{cases}$$

Then, c must necessarily satisfy the resulting EL equation,

$$-(1-c) - a_1\,c'' + a_2\,c^{(4)} - a_3\,c^{(6)} = 0, \quad \text{for all } x \in \Omega,$$

subject to the continuity and remote conditions.

For convenience, we make the change of variable $y = x/\ell_0$. Because c is an even function, we can consider the derivatives for just $y > 0$ and let $y \to 0^+$ to invoke the continuity conditions. We have,

$$c(y) = 1 - \exp(-ky)\Big[c_0 + c_1\, y + c_2\, y^2\Big]$$

$$c'(y) = \exp(-ky)\Big[(-c_1 + k) + (-2c_2 + c_1 k)\, y + (c_2 k)\, y^2\Big]$$

$$c''(y) = \exp(-ky)\Big[(-2c_2 + k^2) + (4c_2 k - k^3)\, y - (c_2 k^2)\, y^2\Big].$$

Hence, the continuity conditions are met if c_0, c_1, and c_2 satisfy the following relations:

$$\boxed{c_0 = 1, \quad c_1 = k, \quad c_2 = \frac{1}{2}k^2}. \tag{2.2}$$

Note that these form the Taylor coefficients.

Let us now solve the EL equation to find a_1, a_2, and a_3. Using the relations (2.2), we find that the derivatives of c are given by (for $y > 0$),

$$c(y) = 1 - \exp(-ky)\Big[1 + (ky) + \frac{1}{2}(ky)^2\Big]$$

$$c'(y) = k\exp(-ky)\Big[\frac{1}{2}(ky)^2\Big]$$

$$c''(y) = k^2\exp(-ky)\Big[(ky) - \frac{1}{2}(ky)^2\Big]$$

$$c'''(y) = k^3\exp(-ky)\Big[1 - 2(ky) + \frac{1}{2}(ky)^2\Big]$$

$$c^{(4)}(y) = k^4\exp(-ky)\Big[-3 + 3(ky) - \frac{1}{2}(ky)^2\Big]$$

$$c^{(5)}(y) = k^5\exp(-ky)\Big[6 - 4(ky) + \frac{1}{2}(ky)^2\Big]$$

$$c^{(6)}(y) = k^6\exp(-ky)\Big[-10 + 5(ky) - \frac{1}{2}(ky)^2\Big].$$

Thus, the EL equation is satisfied, if and only if,

$$-\Big[1 + (ky) + \frac{1}{2}(ky)^2\Big] - \frac{a_1 k^2}{\ell_0^2}\Big[(ky) - \frac{1}{2}(ky)^2\Big] + \frac{a_2 k^4}{\ell_0^4}\Big[-3 + 3(ky) - \frac{1}{2}(ky)^2\Big] - \frac{a_3 k^6}{\ell_0^6}\Big[-10 + 5(ky) - \frac{1}{2}(ky)^2\Big] = 0,$$

or collecting the like terms,

$$\Big[-1 - \frac{3k^4}{\ell_0^4}\, a_2 + \frac{10k^6}{\ell_0^6}\, a_3\Big] + \Big[-1 - \frac{k^2}{\ell_0^2}\, a_1 + \frac{3k^4}{\ell_0^4}\, a_2 - \frac{5k^6}{\ell_0^6}\, a_3\Big](ky) + \Big[-\frac{1}{2} + \frac{k^2}{2\ell_0^2}\, a_1 - \frac{k^4}{2\ell_0^4}\, a_2 + \frac{k^6}{2\ell_0^6}\, a_3\Big](ky)^2 = 0.$$

Since this must hold for every $y > 0$, each of the three bracket terms must identically equal to 0. We get three equations and can solve for a_1, a_2, and a_3:

$$\boxed{a_1 = \frac{3\ell_0^2}{k^2}, \quad a_2 = \frac{3\ell_0^4}{k^4}, \quad a_3 = \frac{\ell_0^6}{k^6}}. \tag{2.3}$$

Note that these form the binomial coefficients.

Finally, let us match the volume integral and the surface integral in 1D. In terms of the normalized coordinate $y = x/\ell_0$, we must have,

$$\int_\Omega \Gamma_{c,6}(y)\, dy = \frac{1}{\ell_0}.$$

Now,

$$\begin{aligned}
\int_\Omega \Gamma_{c,6}(y)\, dy &= 2 \times \frac{1}{4\ell_0} \int_0^\infty \Big[(1-c)^2 + \frac{3}{k^2}(c')^2 + \frac{3}{k^4}(c'')^2 + \frac{1}{k^6}(c''')^2\Big]\, dy \\
&\overset{y \leftarrow ky}{=} \frac{1}{2k\ell_0} \int_0^\infty \Bigg[\Big(1 + y + \frac{1}{2}y^2\Big)^2 + 3\Big(\frac{1}{2}y^2\Big)^2 + 3\Big(y - \frac{1}{2}y^2\Big)^2 \\
&\qquad\qquad + \Big(1 - 2y + \frac{1}{2}y^2\Big)^2\Bigg] \exp(-2y)\, dy \\
&= \frac{1}{2k\ell_0} \underbrace{\int_0^\infty \Big[2 - 2y + 10y^2 - 4y^3 + 2y^4\Big] \exp(-2y)\, dy}_{=3} \\
&= \frac{3}{2k\ell_0}.
\end{aligned}$$

Hence, we must set

$$\boxed{k = \frac{3}{2}}. \tag{2.4}$$

We combine the results (2.2), (2.3), (2.4) with (2.1) to conclude that the phase field and the crack density are given by,

$$\boxed{\begin{aligned}
c(x) &= 1 - \exp\Big(-\frac{3}{2}\frac{|x|}{\ell_0}\Big)\Big[1 + \frac{3}{2}\frac{|x|}{\ell_0} + \frac{9}{8}\frac{|x|^2}{\ell_0^2}\Big] \\
\Gamma_{c,6} &= \frac{1}{4\ell_0}\Big[(1-c)^2 + \frac{4\ell_0^2}{3}(c')^2 + \frac{16\ell_0^4}{27}(c'')^2 + \frac{64\ell_0^6}{729}(c''')^2\Big]
\end{aligned}}. \tag{2.5}$$

We refer to this as the **sixth-order theory**. Again, due to the uniqueness of the solution and the convexity of the crack density, the phase field is the unique global minimizer to the crack density functional.

2.2. Eighth-Order Theory

Suppose now that the phase field c and the crack density $\Gamma_{c,8}$ are given by,

$$\boxed{\begin{aligned} c(x) &= 1 - \exp\Big(-k\,\frac{|x|}{\ell_0}\Big)\Big[c_0 + c_1\,\frac{|x|}{\ell_0} + c_2\,\frac{|x|^2}{\ell_0^2} + c_3\,\frac{|x|^3}{\ell_0^3}\Big] \\ \Gamma_{c,8} &= \frac{1}{4\ell_0}\Big[(1-c)^2 + a_1\,(c')^2 + a_2\,(c'')^2 + a_3\,(c''')^2 + a_4\,(c^{(4)})^2\Big]. \end{aligned}} \tag{2.6}$$

Like before, we must determine the constants $k > 0$, $\{c_0,\, c_1,\, c_2,\, c_3\}$, $\{a_1,\, a_2,\, a_3,\, a_4\}$.

Assume that the phase field solves the minimization problem,

$$\begin{aligned} &\text{minimize} \quad \int_\Omega \Gamma_{c,8}\; dx \\ &\text{subject to} \quad \begin{cases} c(0),\, c'(0),\, c''(0),\, c'''(0) = 0 \\ c(x) \to 1,\; c'(x),\, c''(x),\, c'''(x) \to 0, \quad \text{as } |x| \to \infty. \end{cases} \end{aligned}$$

Then, c necessarily satisfies the EL equation,

$$-(1-c) - a_1\,c'' + a_2\,c^{(4)} - a_3\,c^{(6)} + a_4\,c^{(8)} = 0, \quad \text{for all } x \in \Omega,$$

subject to the continuity and remote conditions.

Again, we make the change of variable $y = x/\ell_0$, and consider the derivatives of c for just $y > 0$. We have,

$$c(y) = 1 - \exp(-ky)\Big[c_0 + c_1\,y + c_2\,y^2 + c_3\,y^3\Big]$$

$$c'(y) = \exp(-ky)\Big[(-c_1 + k) + (-2c_2 + c_1 k)\,y + (-3c_3 + c_2 k)\,y^2 + (c_3 k)\,y^3\Big]$$

$$c''(y) = \exp(-ky)\Big[(-2c_2 + k^2) + (-6c_3 + 4c_2 k - k^3)\,y + (6c_3 k - c_2 k^2)\,y^2 - (c_3 k^2)\,y^3\Big]$$

$$c'''(y) = \exp(-ky)\Big[(-6c_3 + k^3) + (18c_3 k - 2k^4)\,y + (-9c_3 k^2 + \frac{1}{2}k^5)\,y^2 + (c_3 k^3)\,y^3\Big].$$

Hence, the continuity conditions are met if c_0, c_1, c_2, and c_3 satisfy the following relations:

$$\boxed{c_0 = 1, \quad c_1 = k, \quad c_2 = \frac{1}{2}k^2, \quad c_3 = \frac{1}{6}k^3}. \tag{2.7}$$

Let us now solve the EL equation to find a_1, a_2, a_3, and a_4. Use the relations (2.7) to write the derivatives of c as follows (for $y > 0$):

$$c(y) = 1 - \exp(-ky)\Big[1 + (ky) + \frac{1}{2}(ky)^2 + \frac{1}{6}(ky)^3\Big]$$

$$c'(y) = k\exp(-ky)\Big[\frac{1}{6}(ky)^3\Big]$$

$$c''(y) = k^2 \exp(-ky)\Big[\frac{1}{2}(ky)^2 - \frac{1}{6}(ky)^3\Big]$$

$$c'''(y) = k^3 \exp(-ky)\Big[(ky) - (ky)^2 + \frac{1}{6}(ky)^3\Big]$$

$$c^{(4)}(y) = k^4 \exp(-ky)\Big[1 - 3(ky) + \frac{3}{2}(ky)^2 - \frac{1}{6}(ky)^3\Big]$$

$$c^{(5)}(y) = k^5 \exp(-ky)\Big[-4 + 6(ky) - 2(ky)^2 + \frac{1}{6}(ky)^3\Big]$$

$$c^{(6)}(y) = k^6 \exp(-ky)\Big[10 - 10(ky) + \frac{5}{2}(ky)^2 - \frac{1}{6}(ky)^3\Big]$$

$$c^{(7)}(y) = k^7 \exp(-ky)\Big[-20 + 15(ky) - 3(ky)^2 + \frac{1}{6}(ky)^3\Big]$$

$$c^{(8)}(y) = k^8 \exp(-ky)\Big[35 - 21(ky) + \frac{7}{2}(ky)^2 - \frac{1}{6}(ky)^3\Big].$$

The EL equation is satisfied, if and only if,

$$\begin{aligned}\Big[-1 + \frac{k^4}{\ell_0^4}\,a_2 - \frac{10k^6}{\ell_0^6}\,a_3 + \frac{35k^8}{\ell_0^8}\,a_4\Big] + \Big[-1 - \frac{3k^4}{\ell_0^4}\,a_2 + \frac{10k^6}{\ell_0^6}\,a_3 - \frac{21k^8}{\ell_0^8}\,a_4\Big](ky) \\ + \Big[-\frac{1}{2} - \frac{k^2}{2\ell_0^2}\,a_1 + \frac{3k^4}{2\ell_0^4}\,a_2 - \frac{5k^6}{2\ell_0^6}\,a_3 + \frac{7k^8}{2\ell_0^8}\,a_4\Big](ky)^2 \\ + \Big[-\frac{1}{6} + \frac{k^2}{6\ell_0^2}\,a_1 - \frac{k^4}{6\ell_0^4}\,a_2 + \frac{k^6}{6\ell_0^6}\,a_3 - \frac{k^8}{6\ell_0^8}\,a_4\Big](ky)^3 = 0.\end{aligned}$$

By linear independence, the EL equation is satisfied for all $y > 0$, if and only if,

$$\boxed{a_1 = \frac{4\ell_0^2}{k^2}, \quad a_2 = \frac{6\ell_0^4}{k^4}, \quad a_3 = \frac{4\ell_0^6}{k^6}, \quad a_4 = \frac{\ell_0^8}{k^8}}. \tag{2.8}$$

Finally, we find k through normalization:

$$\begin{aligned}\int_\Omega \Gamma_{c,8}(y)\,dy &\overset{y \leftarrow ky}{=} \frac{1}{2k\ell_0}\int_0^\infty \Big[\Big(1 + y + \frac{1}{2}y^2 + \frac{1}{6}y^3\Big)^2 + 4\Big(\frac{1}{6}y^3\Big)^2 + 6\Big(\frac{1}{2}y^2 - \frac{1}{6}y^3\Big)^2 \\ &\qquad + 4\Big(y - y^2 + \frac{1}{6}y^3\Big)^2 + \Big(1 - 3y + \frac{3}{2}y^2 - \frac{1}{6}y^3\Big)\Big]\exp(-2y)\,dy \\ &= \frac{1}{2k\ell_0}\underbrace{\int_0^\infty \Big[2 - 4y + 18y^2 - 16y^3 + \frac{32}{3}y^4 - \frac{8}{3}y^5 + \frac{4}{9}y^6\Big]\exp(-2y)\,dy}_{=4} \\ &= \frac{2}{k\ell_0}.\end{aligned}$$

Hence, we set

$$\boxed{k = 2}. \tag{2.9}$$

The phase field and the crack density are as follows:

$$\boxed{\begin{aligned} c(x) &= 1 - \exp\Big(-2\,\frac{|x|}{\ell_0}\Big)\Big[1 + 2\,\frac{|x|}{\ell_0} + 2\,\frac{|x|^2}{\ell_0^2} + \frac{4}{3}\,\frac{|x|^3}{\ell_0^3}\Big] \\ \Gamma_{c,8} &= \frac{1}{4\ell_0}\Big[(1-c)^2 + \ell_0^2\,(c')^2 + \frac{3\ell_0^4}{8}\,(c'')^2 + \frac{\ell_0^6}{16}\,(c''')^2 + \frac{\ell_0^8}{256}\,(c^{(4)})^2\Big] \end{aligned}} \tag{2.10}$$

We refer to this as the **eighth-order theory**.

2.3. Comparison of Phase Field Models

Let us graph the phase fields, and see how they look differently from one another. We normalize the coordinate and use $y = x/\ell_0$ to claim that any difference among the graphs is independent of the parameter ℓ_0.

Figure 2.1 shows that, when we impose higher continuity in the phase field at a crack, the phase field does look smoother about the crack. As we increase the regularity, the phase field requires "more room" to get away from the value of 0 outside of the crack, but does transition quicker to the value of 1 once it does so.

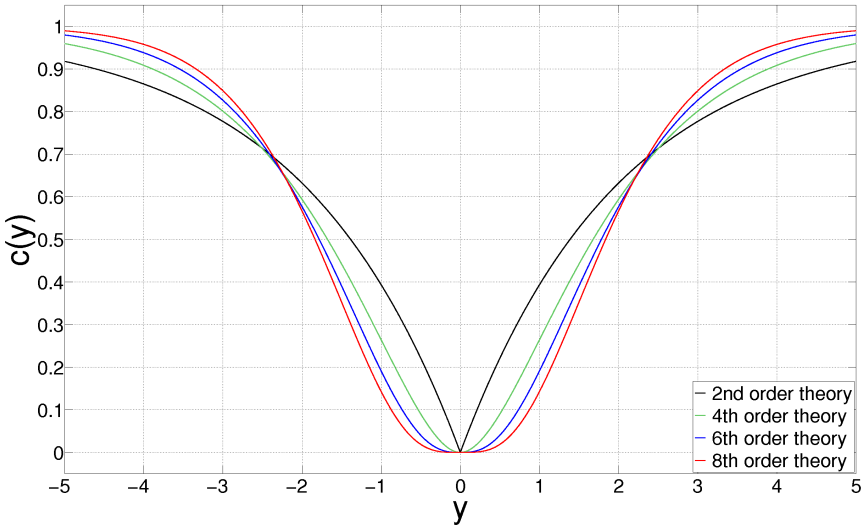

FIGURE 2.1. Phase fields from various theories. See (1.5), (1.7), (2.5), and (2.10).

2.4. Governing Equations

We have examined a specific problem in 1D to find the crack density for each theory. Now that we have the crack densities, we can consider the potential energy (1.4) again and find the EL equations for the general case. These equations govern, not only *what* the displacement and phase fields should be at a given space and time, but also *how* they should in the presence of the other. Here, we will simply list the equations. For an illustration on deriving them carefully, we refer to Section 2.6.

Of course, our discussion is currently limited to the quasi-static, brittle fracture of an elastic material. However, we can always change the energy functional in accordance with a particular theory (e.g. modify the strain energy for hyperelasticity, plasticity, or large deformation, add kinetic energy for dynamics, add thermal energy for temperature-dependence, etc.), write down the governing equations, and numerically solve them to see how well the phase field theory works in a particular setting.

For a linearly elastic material, the strain tensor and the displacement vector are related by the equation,

$$\varepsilon = \frac{\nabla \vec{u} + (\nabla \vec{u})^T}{2}.$$

Furthermore, we assume that the stress and strain tensors are linearly related through a fourth-order, stiffness tensor $\mathbf{C}$:

$$\sigma = \mathbf{C}\varepsilon.$$

We only assume major and minor symmetries for $\mathbf{C}$, i.e. the material does not need to be an isotropic material. The elastic strain energy is given by,

$$\psi_e = \frac{1}{2}\,\sigma : \varepsilon.$$

Second-order theory

Find $(\vec{u},\, c)$ that solves,

$$\begin{cases} -\nabla \cdot (c^2 \sigma) = 0, \\ 2c\,\psi_e + \dfrac{G_c}{2\ell_0}\Big[-(1-c) - 4\ell_0^2\, c''\Big] = 0, \ \text{ in } \Omega. \end{cases}$$

Displacement and tractions are prescribed on the boundary $\partial\Omega$ as usual. In addition, we have Dirichlet BCs for the phase field:

$$c(x) = 1, \ \text{ on } \partial\Omega.$$

It may sound strange that the phase field has Dirichlet BCs to satisfy. Mathematically, however, we must have them if we are to properly define an admissible variation of c. Physically, we are requiring that the body does not just "disintegrate" or "vanish" from the outside due to fracture.

Second-order theory (cont.)

Since the phase field equation is second-order, we must provide two constraints for the phase field (otherwise, the equation is not well-posed). One is the BC stated above. The other is the continuity condition across the crack surface:

$$c(x) = 0, \;\; \text{on } \Gamma_{\text{crack}}.$$

We have a dilemma. This equation is certainly true for points in Γ_{crack}, but we do not know what Γ_{crack} is. After all, we are trying to represent it using the phase field. So this constraint suffers from a circular logic.

For the moment, we will ignore the continuity condition. We will see the ill effect that this has in our numerical simulations, and we will then try to fix it by considering a different constraint.

Fourth-order theory

Find $(\vec{u},\, c)$ that solves,

$$\begin{cases} -\nabla \cdot (c^2 \sigma) = 0, \\ 2c\,\psi_e + \dfrac{G_c}{2\ell_0}\Big[-(1-c) - 2\ell_0^2\, c'' + \ell_0^4\, c^{(4)}\Big] = 0, \;\; \text{in } \Omega. \end{cases}$$

Displacement and tractions are prescribed on the boundary $\partial\Omega$ as usual. For the phase field, we have the Dirichlet BCs,

$$c(x) = 1, \;\; c'(x) = 0, \;\; \text{on } \partial\Omega,$$

and the continuity conditions,

$$c(x) = 0, \;\; c'(x) = 0, \;\; \text{on } \Gamma_{\text{crack}}.$$

Sixth-order theory

Find $(\vec{u},\, c)$ that solves,

$$\begin{cases} -\nabla \cdot (c^2 \sigma) = 0, \\ 2c\,\psi_e + \dfrac{G_c}{2\ell_0}\Big[-(1-c) - \dfrac{4\ell_0^2}{3}\, c'' + \dfrac{16\ell_0^4}{27}\, c^{(4)} - \dfrac{64\ell_0^6}{729}\, c^{(6)}\Big] = 0, \;\; \text{in } \Omega. \end{cases}$$

Displacement and tractions are prescribed on the boundary $\partial\Omega$ as usual. For the phase field, we have the Dirichlet BCs,

$$c(x) = 1, \;\; c'(x) = 0, \;\; c''(x) = 0, \;\; \text{on } \partial\Omega,$$

and the continuity conditions,

$$c(x) = 0, \;\; c'(x) = 0, \;\; c''(x) = 0, \;\; \text{on } \Gamma_{\text{crack}}.$$

Eighth-order theory

Find $(\vec{u},\, c)$ that solves (in Ω),

$$\begin{cases} -\nabla\cdot(c^2\sigma) = 0, \\ 2c\,\psi_e + \dfrac{G_c}{2\ell_0}\Big[-(1-c) - \ell_0^2\,c'' + \dfrac{3\ell_0^4}{8}\,c^{(4)} - \dfrac{\ell_0^6}{16}\,c^{(6)} + \dfrac{\ell_0^8}{256}\,c^{(8)}\Big] = 0. \end{cases}$$

Displacement and tractions are prescribed on the boundary $\partial\Omega$ as usual. For the phase field, we have the Dirichlet BCs,

$$c(x) = 1,\;\; c'(x) = 0,\;\; c''(x) = 0,\;\; c'''(x) = 0,\;\; \text{on } \partial\Omega,$$

and the continuity conditions,

$$c(x) = 0,\;\; c'(x) = 0,\;\; c''(x) = 0,\;\; c'''(x) = 0,\;\; \text{on } \Gamma_{\text{crack}}.$$

2.5. Remarks

For simplicity, we used the prime notation to mark the derivatives of c in the governing equations in 3D. In the domain Ω, we really mean,

$$c'' \equiv \sum_{i=1}^{3} \partial_i^2 c = \Big(\frac{\partial^2 c}{\partial x^2} + \frac{\partial^2 c}{\partial y^2} + \frac{\partial^2 c}{\partial z^2}\Big)$$

$$c^{(4)} \equiv \sum_{i,j=1}^{3} \partial_i^2\partial_j^2 c = \Big(\frac{\partial^4 c}{\partial x^4} + \frac{\partial^4 c}{\partial y^4} + \frac{\partial^4 c}{\partial z^4}\Big) + 2\Big(\frac{\partial^4 c}{\partial x^2\partial y^2} + \frac{\partial^4 c}{\partial x^2\partial z^2} + \frac{\partial^4 c}{\partial y^2\partial z^2}\Big)$$

$$c^{(6)} \equiv \sum_{i,j,k=1}^{3} \partial_i^2\partial_j^2\partial_k^2 c = \cdots$$

$$c^{(8)} \equiv \sum_{i,j,k,l=1}^{3} \partial_i^2\partial_j^2\partial_k^2\partial_l^2 c = \cdots,$$

and on the boundaries $\partial\Omega$ and Γ_{crack} (that has an outward, unit normal $\vec{n}$), we mean,

$$c' \equiv (\nabla c)\cdot\vec{n}$$

$$c'' \equiv$$

$$c''' \equiv$$

2.6. Appendix for Section 2

$$\Psi(u,\,c)=\int_\Omega c^2\,\frac{1}{2}E(u')^2\;dx+\int_\Omega\frac{G_c}{4\ell_0}\Big[(1-c)^2+\frac{4\ell_0^2}{3}\,(c')^2+\frac{16\ell_0^4}{27}\,(c'')^2+\frac{64\ell_0^6}{729}\,(c''')^2\Big]\;dx.$$

Suppose that $(u,\,c)$ minimizes Ψ. Then, the perturbed energy $\Psi_\epsilon\equiv\Psi(u+\epsilon v,\,c+\epsilon d)$, due to a variation $\epsilon(v,\,d)\equiv(\epsilon v,\,\epsilon d)$, has a minimum when $\epsilon=0$. Hence,

$$\frac{d\Psi_\epsilon}{d\epsilon}\Big|_{\epsilon=0}\equiv\Big[\frac{d}{d\epsilon}\Psi(u+\epsilon v,\,c+\epsilon d)\Big]_{\epsilon=0}=0,\quad\text{for all admissible }(v,\,d).$$

Now,

$$\begin{aligned}\frac{d\Psi_\epsilon}{d\epsilon}&=\int_\Omega\Big[(c+\epsilon d)^2\cdot E(u'+\epsilon v')v'+2(c+\epsilon d)d\cdot\frac{1}{2}E(u')^2\Big]\;dx\\&\quad+\int_\Omega\frac{G_c}{2\ell_0}\Big[(1-c-\epsilon d)(-d)+\frac{4\ell_0^2}{3}(c'+\epsilon d')d'\\&\qquad+\frac{16\ell_0^4}{27}(c''+\epsilon d'')d''+\frac{64\ell_0^6}{729}(c'''+\epsilon d''')d'''\Big]\;dx.\end{aligned}$$

Set $\epsilon=0$ to get,

$$\begin{aligned}\frac{d\Psi_\epsilon}{d\epsilon}\Big|_{\epsilon=0}&=\int_\Omega\Big[c^2Eu'v'+2cd\cdot\frac{1}{2}E(u')^2\Big]\;dx\\&\quad+\int_\Omega\frac{G_c}{2\ell_0}\Big[-(1-c)d+\frac{4\ell_0^2}{3}c'd'+\frac{16\ell_0^4}{27}c''d''+\frac{64\ell_0^6}{729}c'''d'''\Big]\;dx.\end{aligned}\tag{2.11}$$

Note, the expression in (2.11) can correspond to the residuals of the governing equations in weak form. We will later use this for FE implementation.

To write the strong form of the governing equations, we integrate the RHS by parts to expose v and d. We do this formally and assume that u and c are sufficiently smooth to take on additional derivatives. Then,

$$\begin{aligned}\frac{d\Psi_\epsilon}{d\epsilon}\Big|_{\epsilon=0}&=\int_\Omega-(c^2Eu')'v\;dx+\Big[c^2Eu'v\Big]_{-\infty}^{\infty}\\&\quad+\int_\Omega\left[2c\cdot\frac{1}{2}E(u')^2+\frac{G_c}{2\ell_0}\Big[-(1-c)-\frac{4\ell_0^2}{3}c''+\frac{16\ell_0^4}{27}c^{(4)}-\frac{64\ell_0^6}{729}c^{(6)}\Big]\right]d\;dx\\&\quad+\underbrace{\frac{G_c}{2\ell_0}\left[\frac{4\ell_0^2}{3}\big[-c'v\big]+\frac{16\ell_0^4}{27}\big[-c''v'+c'''v\big]+\frac{64\ell_0^6}{729}\big[-c'''v''+c^{(4)}v'-c^{(5)}v\big]\right]_{-\infty}^{\infty}}_{(*)}.\end{aligned}$$

Let us examine the boundary term $(*)$. Previously, we imposed remote conditions (really BCs) on c, c', and c''. In return, an admissible d satisfied $d(x)=0$, $d'(x)=0$, and $d''(x)=0$ on the boundary, and the boundary term $(*)$ vanished for all d.

3. Three Model Problems in 1D

Let us now derive the strong form, which will relate the displacement and phase fields. To specify a degradation in stress when the body is in tension but not in compression, we decompose the elastic strain energy density ψ_e into a tensile and a compressive part based on the eigenvalues of the strain tensor ε (see [1], [4]):

$$\psi_e = g(c)\psi_e^+ + \psi_e^-.$$

The function $g = g(c) \in [0, 1]$ is called the **degradation function**, and it satisfies the properties $g(0) = 0$, $g(1) = 1$, and $g'(0) = 0$. Note, the arguments in g here are not the constant zero and one functions, but the evaluations of the phase field at a point. In other words, these properties hold when we have $c(x) = 0$ or $c(x) = 1$ at x, i.e. when the material is fully damaged or undamaged at x. For our simulations, we considered the quadratic function $g(c) = c^2$. However, we allow any increasing function with the properties above, such as a cubic function $g(c) = 3c^2 - 2c^3$.

By taking the variational derivative of (1.3) with respect to $\vec{u}$ and to c, we obtain the strong form:

Find $\{\vec{u}, c\}$ that solves

$$\begin{cases} -\nabla \cdot \sigma = \vec{0} \\ g'(c)\psi_e^+ + G_c \delta c = 0 \end{cases} \quad \text{in } \Omega \setminus \Gamma, \tag{3.1}$$

subject to Dirichlet and Neumann BCs on $\partial\Omega$.

We see that we have to solve a coupled equation that is, in general, nonlinear in c. Note, $g'(c) = 2c$ for the quadratic degradation function, and δc denotes the variational derivative of $\int \Gamma_c \, dx$ with respect to c, i.e. what we usually do to get the EL equation. For simplicity, we omitted the body force and acceleration in the momentum equation. We will refer to the second equation as the phase field equation.

Consider a 1D bar of length $2L$ ($\Omega = (-L, L)$), with a crack in the middle $x = 0$. We fix the left end of the bar, and pull the right end by a displacement of $u_0 > 0$. In this purely tensile problem, $\psi_e^- = 0$, and we have

$$\psi_e^+ = \frac{1}{2} E(u')^2, \quad \sigma = g(c)\varepsilon = c^2 E u'.$$

Hence, we seek $\{u, c\}$ that solves,

$$\begin{cases} -(c^2 E u')' = 0 \\ cE(u')^2 + G_c \delta c = 0 \end{cases} \quad \text{in } (-L, L) \setminus \{0\}. \tag{3.2}$$

The Dirichlet BCs for u remain the same—namely, $u(-L) = 0$ and $u(L) = u_0$—but the Neumann BCs for c differ for each theory. We will list these later.

First, we will decouple (3.2) and examine the two equations separately. We will then solve the coupled problem. For all three problems, we will use the following parameters:

$$L = 100, \quad E = 10^6, \quad G_c = 1, \quad u_0 = 0.1, \quad \ell_0 = 1/8.$$

3.1. Problem 1: Finding the Displacement Field Only

Given a phase field c from one of the theories, how close is the finite element (FE) solution of the displacement field, u_h, resulting from

$$-(c^2 E u_h')' = 0 \tag{3.3}$$

to the analytical solution u (a discontinuous, piecewise constant function)?

Following the isogeometric analysis approach, we will use B-spline basis functions to model the displacement field. The analytical solutions in (1.4), (1.6), (2.6), (2.10), (**??**), and (**??**) will be used for the phase field. So the only things that can effect a discrepancy in the results are the degree of the B-splines (smoothness of the basis functions) and the expression of the phase field (smoothness at the crack $x = 0$).

Let $numElems$ denote the number of elements used to discretize the domain $[-L,\, L]$, and p the degree of the B-splines. We will then have $n = (numElems{+}p)$ basis functions. Adhering to the notations of IGA, we denote these basis functions by $\{N_1,\, N_2,\, \cdots,\, N_n\}$. Then, we can write our FE solution of the displacement field as,

$$u_h(x) = \sum_{B=1}^{n} u_B N_B(x),$$

where $\{u_1,\, u_2,\, \cdots,\, u_n\}$ are the unknown coefficients.

The knot vector Ξ that creates the B-splines is open and uniform over the parametric domain, [0, 1]. For example, with $numElems = 10$ and $p = 2$,

$$\Xi = \big(\overbrace{0.0,\ 0.0,}^{p \text{ times}}\ \underbrace{0.0,\ 0.1,\ 0.2,\ \cdots,\ 0.9,\ 1.0,}_{\text{increment of } 1/numElems}\ \overbrace{1.0,\ 1.0}^{p \text{ times}}\big).$$

Since the knot vector is open, we already know from the BCs that $u_1 = 0$ and $u_n = u_0$. Hence, there are $(n - 2)$ unknowns that we need to find. The internal knot values are uniformly spaced apart, so we will let $h = (2L/numElems)$ represent the mesh size.

In our simulation, we solved the momentum equation with 4000, 8000, 16000, 32000, and 64000 elements. For the second-order theory, we used linear B-splines; for fourth-order, quadratic; for sixth-order, cubic; and for eighth-order, quartic.

Figures 3.1–3.6 show what the solution u_h looks like for the various theories, and how it converges to the analytical solution as we h-refine the mesh. Note that the horizontal axis represents the physical domain $[-100,\, 100]$ and we are focusing on a small part near the crack $x = 0$ to see the interesting behaviors.

We immediately see that the second-order theory gives us the worst profile of the displacement field. Even with 64000 elements, the solution does not immediately reach the two values 0 and u_0 away from the crack. (It is difficult to imagine from this plot, but the solution does reach 0 and u_0 at $x = \pm 100$—just not before.)

The displacement field from the higher-order theories does look better, and the sixth- and eighth-order theories give us a better profile than their alternative counterparts do. However, there are slight undershoot and overshoot in u_h near the crack. This may be attributed to the smoothness that we required of u_h (of the basis functions).

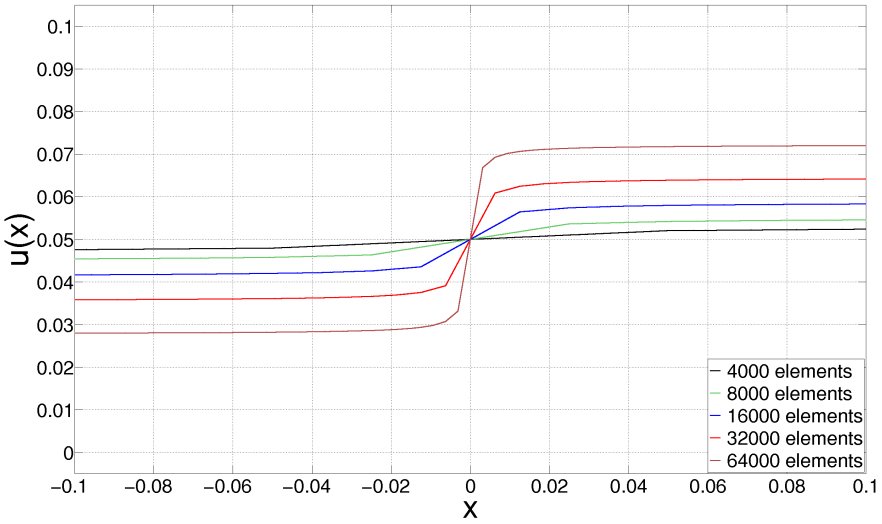

FIGURE 3.1. The displacement field from the second-order theory (decoupled).

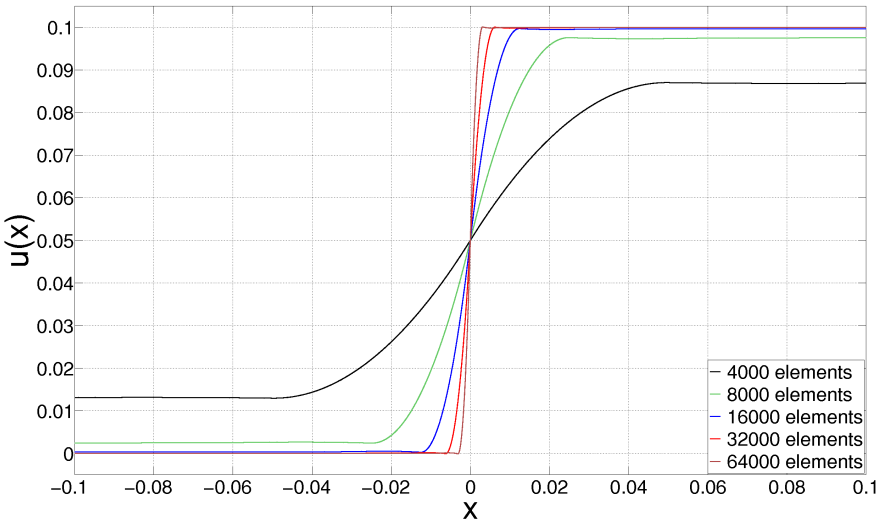

FIGURE 3.2. The displacement field from the fourth-order theory (decoupled).

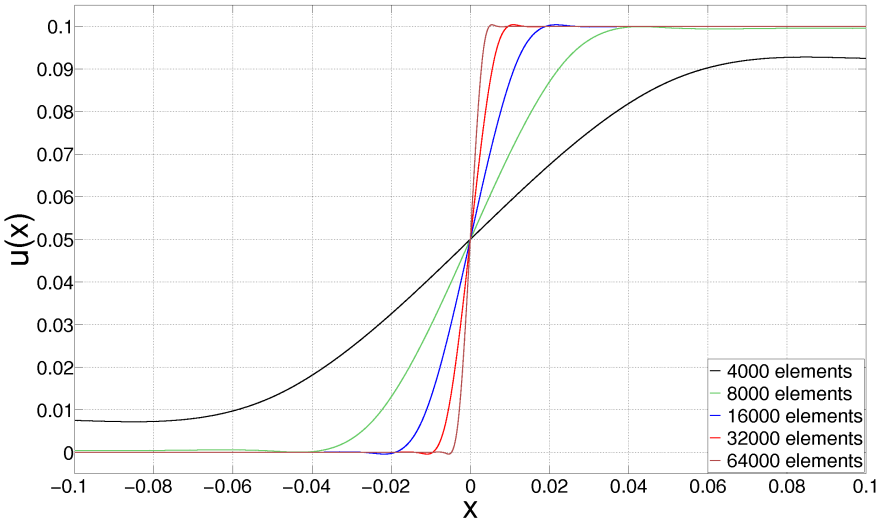

FIGURE 3.3. The displacement field from the sixth-order theory (decoupled).

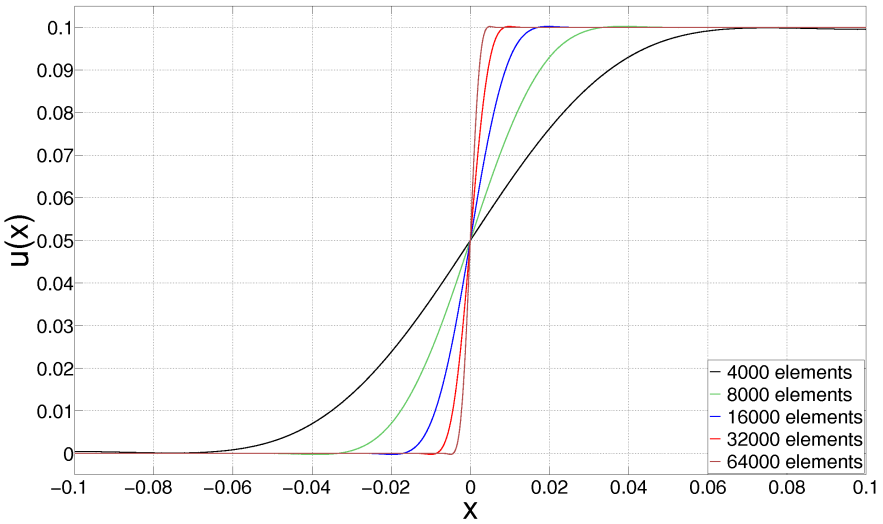

FIGURE 3.4. The displacement field from the eighth-order theory (decoupled).

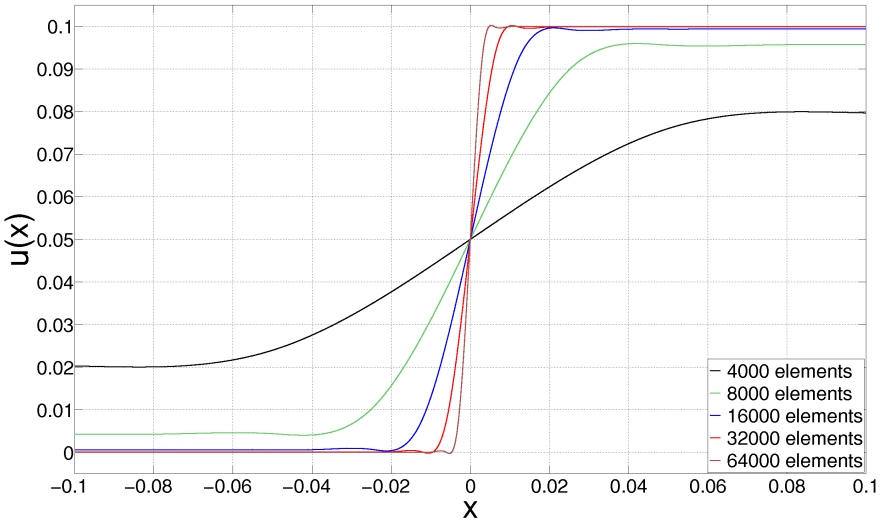

FIGURE 3.5. The displacement field from the alternative sixth-order theory (decoupled).

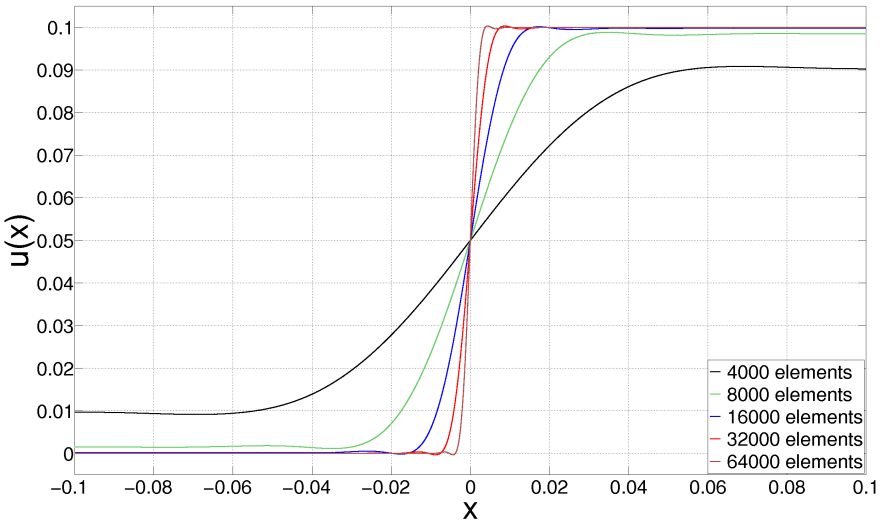

FIGURE 3.6. The displacement field from the alternative eighth-order theory (decoupled).

To quantify how good our theories are, we consider the strain energy error between the displacements u and u_h. For this problem,

$$\boxed{\text{strain energy error} = \frac{1}{2}\int_{-L}^{L} c^2 E(u_h')^2 \, dx}. \tag{3.4}$$

Note, we used the facts that u' is zero almost everywhere and $c(0) = 0$ for all the theories. The latter means, despite the discontinuity of u' at $x = 0$, the integral can be considered well-defined.

The log-log plot in Figure 3.7 shows that the strain energy error converges to 0 faster for the higher-order theories. However, the alternative sixth- and eighth-order theories can converge no faster than the fourth-order theory can. We will validate these two observations by proving a priori estimates in the next section.

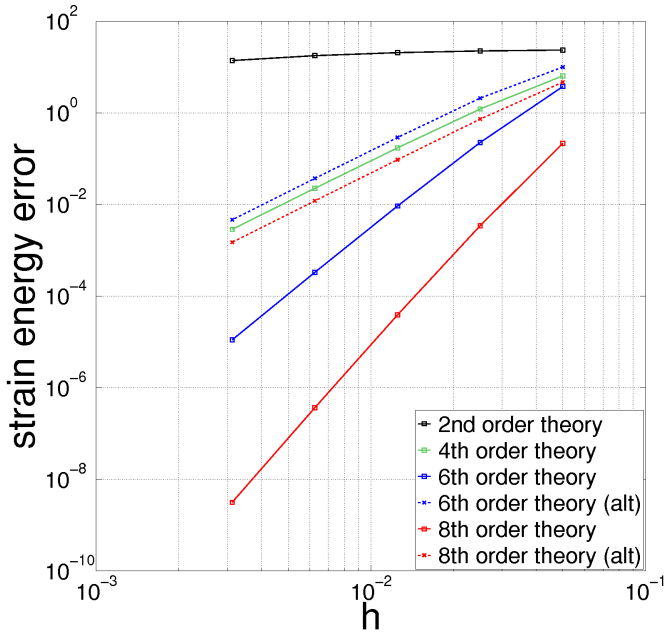

FIGURE 3.7. The strain energy errors are plotted against the mesh size.

What happens if we fix the degree of the B-splines to be the same (quartic) for all the theories? Figure 3.8 shows that, barring a constant factor, the errors still converge at the same rates. There does not seem to be an advantage to use a higher degree for the basis functions than that required. But moreover, we may now attribute the discrepancy in the rates of convergence to the smoothness of the phase field.

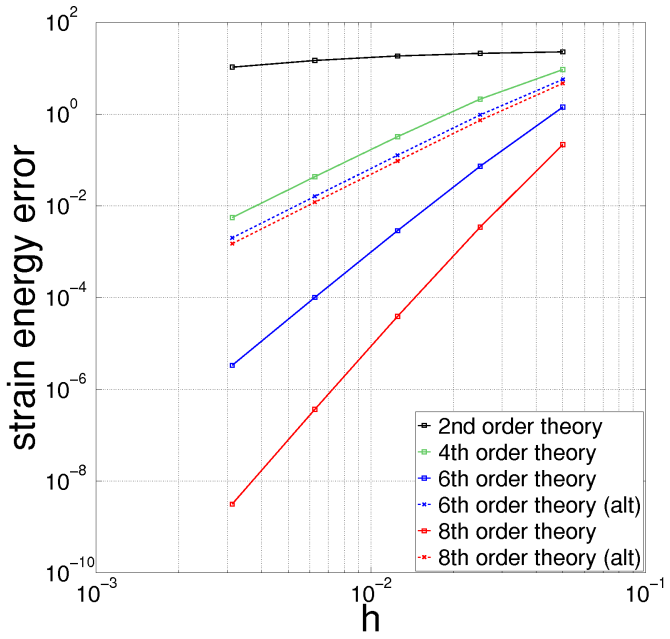

FIGURE 3.8. The strain energy errors still converge at the same rates if the degree of the B-splines is higher than that required.

3.1.1. A Priori Estimate of the Strain Energy Error

We can use the best approximation theorem for the Galerkin method to study the convergence rate of the strain energy error. For clarity, we use $|u-u_h|_e$ here to denote the error between u and u_h. Let S_h be the space of test and trial functions (the B-splines). Then, the best approximation theorem says,

$$|u - u_h|_e \leq |u - w_h|_e, \text{ for all } w_h \in S_h.$$

Since any spline can be written as a linear combination of B-splines, the idea is to select a piecewise polynomial with sufficient continuity for w_h, so that we have an upper bound for the strain energy error. We will see that the upper bound depends on the mesh size h, and also on the model parameters. When compared against the convergence plots in Figure 3.7, we find that these upper bounds are almost tight.

We summarize the results for the second- and fourth-order theories here. The next page will show how to derive such results for the sixth- and eighth-order theories.

For the second-order theory, S_h is the set of linear B-splines. Let $w_h \in S_h$ be a C^0, piecewise linear function as follows:

$$w_h(x) = \begin{cases} 0, & \text{if } x \in [-L, -\epsilon] \\ \dfrac{u_0}{2\epsilon}(x+\epsilon), & \text{if } x \in [-\epsilon, \epsilon] \\ u_0, & \text{if } x \in [\epsilon, L] \end{cases} . \tag{3.5}$$

The parameter ϵ determines how quickly we can transition from 0 to u_0 without letting w_h "go outside" the space S_h. Here, $\epsilon = h$, the mesh size.

We find that,

$$\boxed{|u - u_h|_e \leq \frac{1}{48} E \Big(\frac{u_0}{\ell_0}\Big)^2 \epsilon}. \tag{3.6}$$

In other words, as we h-refine the mesh, the error converges at a rate of 1.

For the fourth-order theory, S_h is the set of quadratic B-splines. Let $w_h \in S_h$ be a C^1, piecewise quadratic function:

$$w_h(x) = \begin{cases} 0, & \text{if } x \in [-L, -\epsilon] \\ \dfrac{u_0}{2\epsilon^2}(x^2 + 2\epsilon x + \epsilon^2), & \text{if } x \in [-\epsilon, 0] \\ \dfrac{u_0}{2\epsilon^2}(-x^2 + 2\epsilon x + \epsilon^2), & \text{if } x \in [0, \epsilon] \\ u_0, & \text{if } x \in [\epsilon, L] \end{cases} . \tag{3.7}$$

Again, $\epsilon = h$. Then, we get

$$\boxed{|u - u_h|_e \leq \frac{1}{420} E \Big(\frac{u_0}{\ell_0^2}\Big)^2 \epsilon^3}. \tag{3.8}$$

Hence, for the fourth-order theory, the error converges at a rate of 3.

We will now prove a priori estimates for the sixth- and eighth-order theories. For the sixth-order theory, S_h is the set of cubic B-splines. So consider this C^2, piecewise cubic function for $w_h \in S_h$ (note that $\epsilon = 3h$):

$$w_h(x) = \begin{cases} 0, & \text{if } x \in [-L,\, -\epsilon] \\ \dfrac{u_0}{16\epsilon^3}(9x^3 + 27\epsilon x^2 + 27\epsilon^2 x + 9\epsilon^3), & \text{if } x \in [-\epsilon,\, -\dfrac{\epsilon}{3}] \\ \dfrac{u_0}{16\epsilon^3}(-18x^3 + 18\epsilon^2 x + 8\epsilon^3), & \text{if } x \in [-\dfrac{\epsilon}{3},\, \dfrac{\epsilon}{3}] \\ \dfrac{u_0}{16\epsilon^3}(9x^3 - 27\epsilon x^2 + 27\epsilon^2 x + 7\epsilon^3), & \text{if } x \in [\dfrac{\epsilon}{3},\, \epsilon] \\ u_0, & \text{if } x \in [\epsilon,\, L] \end{cases} . \tag{3.9}$$

Then, by the best approximation theorem,

$$\begin{aligned} |u - u_h|_e &\le \frac{E}{2} \int_{-L}^{L} c^2 (w_h')^2 \, dx \\ &= 2 \times \frac{E}{2} \Big(\frac{u_0}{16\epsilon^3} \Big)^2 \left[\int_0^{\epsilon/3} c(x)^2 (-54x^2 + 18\epsilon^2)^2 \, dx + \int_{\epsilon/3}^{\epsilon} c(x)^2 (27x^2 - 54\epsilon x + 27\epsilon^2)^2 \, dx \right], \end{aligned}$$

and we can focus on the interval $[0,\, \epsilon]$ to examine the phase field c.

Recall the phase field (2.6) and consider its Taylor expansion about $x = 0$:

$$\begin{aligned} c(x) &= 1 - \exp\Big(-\frac{3}{2}\frac{x}{\ell_0}\Big)\Big[1 + \frac{3}{2}\frac{x}{\ell_0} + \frac{9}{8}\frac{x^2}{\ell_0^2}\Big] \\ &= 1 - \left[1 - \frac{3}{2}\frac{x}{\ell_0} + \frac{1}{2}\Big(\frac{3}{2}\frac{x}{\ell_0}\Big)^2 - \frac{1}{6}\Big(\frac{3}{2}\frac{x}{\ell_0}\Big)^3 + \frac{1}{24}\Big(\frac{3}{2}\frac{x}{\ell_0}\Big)^4 - \cdots\right]\Big[1 + \frac{3}{2}\frac{x}{\ell_0} + \frac{9}{8}\frac{x^2}{\ell_0^2}\Big] \\ &= \frac{9}{16}\frac{x^3}{\ell_0^3} - \frac{81}{128}\frac{x^4}{\ell_0^4} + \frac{243}{640}\frac{x^5}{\ell_0^5} - \cdots . \end{aligned}$$

Since ϵ is supposed to be small, we can take the first two terms to say that

$$c(x) \le \frac{9}{16}\frac{x^3}{\ell_0^3}, \text{ for all } x \in [0,\, \epsilon].$$

The integrands are nonnegative, so we can bound the strain energy error from above by,

$$\begin{aligned} |u - u_h|_e &\le E\Big(\frac{u_0}{16\epsilon^3}\Big)^2 \left[\int_0^{\epsilon/3} \Big(\frac{9}{16}\frac{x^3}{\ell_0^3}\Big)^2 (-54x^2 + 18\epsilon^2)^2 \, dx \right. \\ &\qquad \left. + \int_{\epsilon/3}^{\epsilon} \Big(\frac{9}{16}\frac{x^3}{\ell_0^3}\Big)^2 (27x^2 - 54\epsilon x + 27\epsilon^2)^2 \, dx \right] \\ &= \boxed{\frac{5527}{14192640} E \Big(\frac{u_0}{\ell_0^3}\Big)^2 \epsilon^5}, \end{aligned} \tag{3.10}$$

and say that the error converges at a rate of 5.

Consider the alternative sixth-order theory now. The Taylor expansion of the phase field (2.10) is given by,

$$c(x) = \frac{8}{27}\frac{x^2}{\ell_0^2} - \frac{32}{243}\frac{x^4}{\ell_0^4} + \frac{1024}{10935}\frac{x^5}{\ell_0^5} - \cdots .$$

Using the same cubic spline for w_h, we can bound the strain energy error from above by,

$$\begin{aligned} |u-u_h|_e \leq E\Big(\frac{u_0}{16\epsilon^3}\Big)^2 \Bigg[&\int_0^{\epsilon/3} \Big(\frac{8}{27}\frac{x^2}{\ell_0^2}\Big)^2 (-54x^2+18\epsilon^2)^2 \, dx \\ &+ \int_{\epsilon/3}^{\epsilon} \Big(\frac{8}{27}\frac{x^2}{\ell_0^2}\Big)^2 (27x^2-54\epsilon x+27\epsilon^2)^2 \, dx \Bigg] \\ = \boxed{\frac{116}{295245} E\Big(\frac{u_0}{\ell_0^2}\Big)^2 \epsilon^3}. \end{aligned} \tag{3.11}$$

We see that the strain energy error converges at a rate of 3 only.

For the eighth-order theory, S_h is the set of quartic B-splines. Consider the following C^3, piecewise quartic function $w_h \in S_h$ (with $\epsilon = 2h$):

$$u(x) = \begin{cases} 0, & \text{if } x \in [-L, -\epsilon] \\ \frac{u_0}{6\epsilon^4}(4x^4+16\epsilon x^3+24\epsilon^2x^2+16\epsilon^3x+4\epsilon^4), & \text{if } x \in [-\epsilon, -\frac{\epsilon}{2}] \\ \frac{u_0}{6\epsilon^4}(-12x^4-16\epsilon x^3+8\epsilon^3x+3\epsilon^4), & \text{if } x \in [-\frac{\epsilon}{2}, 0] \\ \frac{u_0}{6\epsilon^4}(12x^4-16\epsilon x^3+8\epsilon^3x+3\epsilon^4), & \text{if } x \in [0, \frac{\epsilon}{2}] \\ \frac{u_0}{6\epsilon^4}(-4x^4+16\epsilon x^3-24\epsilon^2x^2+16\epsilon^3x+2\epsilon^4), & \text{if } x \in [\frac{\epsilon}{2}, \epsilon] \\ u_0, & \text{if } x \in [\epsilon, L] \end{cases} . \tag{3.12}$$

Then, we have,

$$\begin{aligned} |u-u_h|_e \leq E\Big(\frac{u_0}{6\epsilon^4}\Big)^2 \Bigg[&\int_0^{\epsilon/2} c(x)^2 (48x^3-48\epsilon x^2+8\epsilon^3)^2 \, dx \\ &+ \int_{\epsilon/2}^{\epsilon} c(x)^2 (-16x^3+48\epsilon x^2-48\epsilon^2x+16\epsilon^3)^2 \, dx \Bigg], \end{aligned}$$

and we can again focus on the interval $[0, \epsilon]$ to look at the phase field c.

Consider the Taylor expansion of the phase field (**??**) about $x = 0$:

$$c(x) = \frac{2}{3}\frac{x^4}{\ell_0^4} - \frac{16}{15}\frac{x^5}{\ell_0^5} + \frac{8}{9}\frac{x^6}{\ell_0^6} - \cdots .$$

Then,

$$|u-u_h|_e \le E\Big(\frac{u_0}{6\epsilon^4}\Big)^2\left[\int_0^{\epsilon/2}\Big(\frac{2}{3}\frac{x^4}{\ell_0^4}\Big)^2(48x^3-48\epsilon x^2+8\epsilon^3)^2\,dx\right.$$
$$\left.+\int_{\epsilon/2}^{\epsilon}\Big(\frac{2}{3}\frac{x^4}{\ell_0^4}\Big)^2(-16x^3+48\epsilon x^2-48\epsilon^2x+16\epsilon^3)^2\,dx\right]$$
$$=\boxed{\frac{16183}{233513280}E\Big(\frac{u_0}{\ell_0^4}\Big)^2\epsilon^7}, \tag{3.13}$$

i.e. the strain energy error converges at a rate of 7.

Finally, let us consider the alternative eighth-order theory. The Taylor expansion of the phase field (**??**) is as follows:

$$c(x)=\frac{32}{125}\frac{x^2}{\ell_0^2}-\frac{512}{9375}\frac{x^4}{\ell_0^4}+\frac{16384}{703125}\frac{x^6}{\ell_0^6}-\cdots.$$

We use the same quartic spline for w_h. This time,

$$|u-u_h|_e \le E\Big(\frac{u_0}{6\epsilon^4}\Big)^2\left[\int_0^{\epsilon/2}\Big(\frac{32}{125}\frac{x^2}{\ell_0^2}\Big)^2(48x^3-48\epsilon x^2+8\epsilon^3)^2\,dx\right.$$
$$\left.+\int_{\epsilon/2}^{\epsilon}\Big(\frac{32}{125}\frac{x^2}{\ell_0^2}\Big)^2(-16x^3+48\epsilon x^2-48\epsilon^2x+16\epsilon^3)^2\,dx\right]$$
$$=\boxed{\frac{29728}{162421875}E\Big(\frac{u_0}{\ell_0^2}\Big)^2\epsilon^3}, \tag{3.14}$$

i.e. the strain energy error converges at a rate of 3 only.

Below, we list the rates of convergence that we obtained from the a priori estimates, and compare them to the ones we had gotten numerically. The errors for 16000, 32000, 64000 elements were used to calculate the slope of the least-squares line.

	rate of convergence	
	theoretical	experimental
2nd-order	1	0.287
4th-order	3	2.950
6th-order	5	4.856
8th-order	7	6.797
alternative 6th-order	3	2.985
alternative 8th-order	3	2.994

3.2. Problem 2: Finding the Phase Field Only

Given a displacement field u, how close is the FE solution of the phase field, c_h, which results from the phase field equation,

$$c_h E(u')^2 + G_c \delta c_h = 0, \tag{3.15}$$

to the analytical solution c?

Again, we model the phase field with B-splines that are generated by an open, uniform knot vector. Hence, if we suppose that there are n basis functions, then,

$$c_h(x) = \sum_{B=1}^{n} c_B N_B(x),$$

where $\{c_1, c_2, \cdots, c_n\}$ are the unknown coefficients. As we will have Neumann BCs for the phase field, there are n unknowns for us to find.

For the displacement field u, we take the spline interpolate that smoothly transitions from 0 to u_0 over the interval $[-\epsilon, \epsilon]$. We refer to (3.5), (3.7), (3.9), and (3.12) for the specific forms that u and the parameter ϵ take for each theory. We let u be a continuous function instead of the discontinuous, piecewise constant function, for we are building our way towards the coupled problem where the FE solution is continuous.

In our simulation, we solved the phase field equation with 4000, 8000, 16000, 32000, and 64000 elements. For the second-order theory, we used linear B-splines; for fourth-order, quadratic; for sixth-order, cubic; and for eighth-order, quartic.

We can find the Neumann BCs as we derive the weak form of the phase field equation. For brevity, we will illustrate this only once for the sixth-order theory.

From the crack density functional $\Gamma_{c,6}$ in (2.6), we see that,

$$\delta c = \frac{1}{2\ell_0}\Big[(c-1) - \frac{4\ell_0^2}{3}c'' + \frac{16\ell_0^4}{27}c^{(4)} - \frac{64\ell_0^6}{729}c^{(6)}\Big].$$

Multiply the phase field equation (3.2) by a test function $v \in H^3\big((-L,\, L)\big)$ and integrate by parts. We get,

$$\int_{-L}^{L} E(u')^2\, cv\; dx + \int_{-L}^{L} \frac{G_c}{2\ell_0}\Big[cv + \frac{4\ell_0^2}{3}c'v' + \frac{16\ell_0^4}{27}c''v'' + \frac{64\ell_0^6}{729}c'''v'''\Big]\; dx$$
$$+ \underbrace{\frac{G_c}{2\ell_0}\left(\frac{4\ell_0^2}{3}\big[-c'v\big]_{-L}^{L} + \frac{16\ell_0^4}{27}\big[-c''v' + c'''v\big]_{-L}^{L} + \frac{64\ell_0^6}{729}\big[-c'''v'' + c^{(4)}v' - c^{(5)}v\big]_{-L}^{L}\right)}_{(*)}$$
$$= \int_{-L}^{L} \frac{G_c}{2\ell_0} v\; dx.$$

Suppose we want the boundary terms in $(*)$ to vanish for all possible v. Then, the solution c must satisfy the following BCs:

$$\begin{cases} -\dfrac{4\ell_0^2}{3}\,c'(L) + \dfrac{16\ell_0^4}{27}\,c'''(L) - \dfrac{64\ell_0^6}{729}\,c^{(5)}(L) = 0, \\ \dfrac{4\ell_0^2}{3}\,c'(-L) - \dfrac{16\ell_0^4}{27}\,c'''(-L) + \dfrac{64\ell_0^6}{729}\,c^{(5)}(-L) = 0, \\ -\dfrac{16\ell_0^4}{27}\,c''(L) + \dfrac{64\ell_0^6}{729}\,c^{(4)}(L) = 0, \\ \dfrac{16\ell_0^4}{27}\,c''(-L) - \dfrac{64\ell_0^6}{729}\,c^{(4)}(-L) = 0, \\ -\dfrac{64\ell_0^6}{729}\,c'''(L) = 0, \\ \dfrac{64\ell_0^6}{729}\,c'''(-L) = 0. \end{cases} \tag{3.16}$$

Since the crack density functional for the alternative sixth-order theory takes the same differential form but has different coefficients, we can just alter the coefficients in (3.16) to get the BCs for the alternative sixth-order theory.

Figures 3.9–3.14 show what the FE solution c_h looks like for the various theories, and how it converges to the analytical solution as we h-refine the mesh. Again, the horizontal axis represents the physical domain $(-100, 100)$ and we are focusing on an area near the crack $x = 0$ to see the interesting behaviors.

For all theories, the FE solution steadily approaches the analytical solution. However, it is apparent that we need more than 64000 elements in the decoupled problem in order for c_h to reach the value of 0 at the crack $x = 0$.

Now, for the sixth- and eighth-order theories, we notice a rather disturbing behavior as we decrease h: the curvatures of c_h and c begin to differ at $x = 0$ (the phase field c_h is not "flat"). Despite the fact that we had specified $c''(0) = 0$ as a continuity condition, the type of Neumann BCs that we imposed on c_h does not reflect this. It seems like the FE solution is converging to a solution that is different from the analytical solution. For the alternative sixth- and eighth-order theories, we do not see this problem.

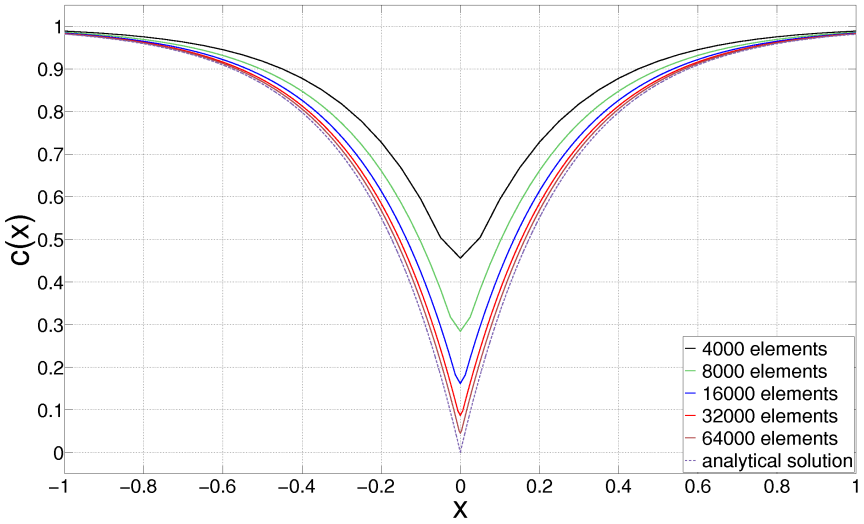

FIGURE 3.9. The phase field from the second-order theory (decoupled).

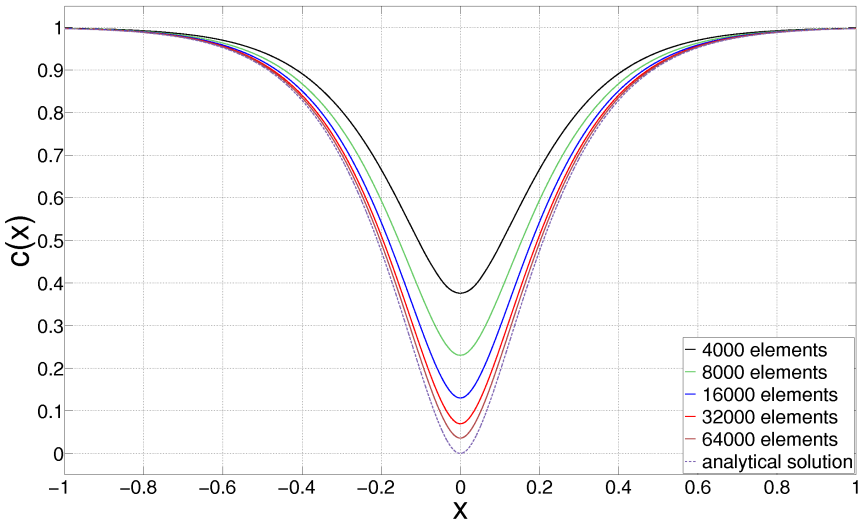

FIGURE 3.10. The phase field from the fourth-order theory (decoupled).

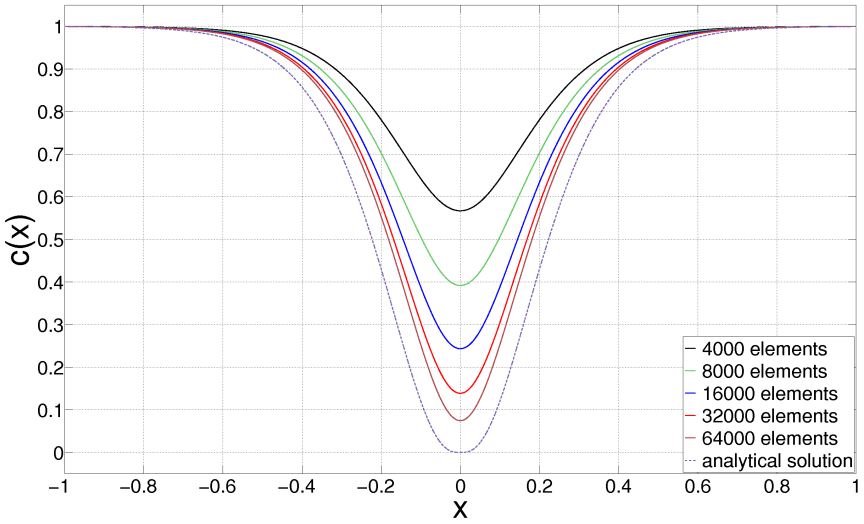

FIGURE 3.11. The phase field from the sixth-order theory (decoupled).

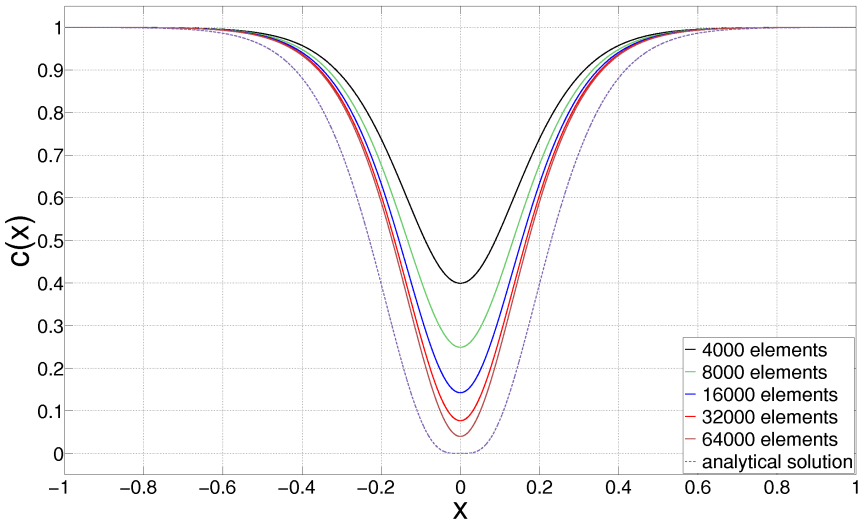

FIGURE 3.12. The phase field from the eighth-order theory (decoupled).

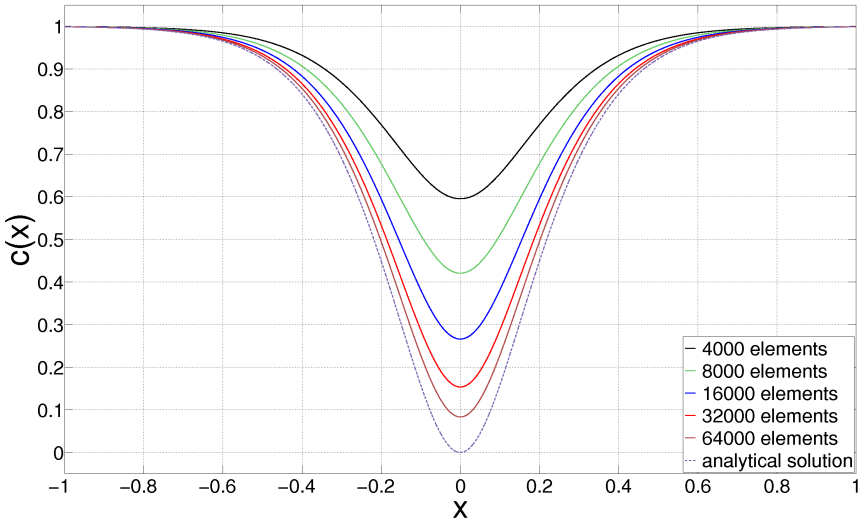

FIGURE 3.13. The phase field from the alternative sixth-order theory (decoupled).

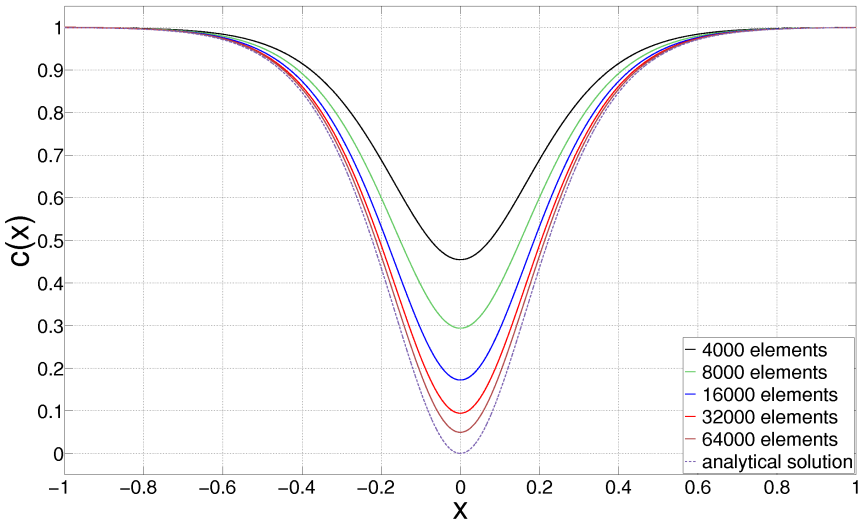

FIGURE 3.14. The phase field from the alternative eighth-order theory (decoupled).

To quantify how good our theories are, we consider the difference between the volume integral and surface integral in (??). We call this the surface energy error between the phase fields c and c_h. For this problem,

$$\boxed{\text{surface energy error} = \left| \left(\int_{-L}^{L} G_c \Gamma_{c_h} \, dx \right) - G_c \right|}. \tag{3.17}$$

We used the fact that the energy to create a new surface is G_c (by definition), in order to bypass the notion that the integral over a point $\Gamma = \{0\}$ is zero.

Figure 3.15 shows that the surface energy errors do converge to 0 for all theories. The rate at which the error diminishes is the same for the second-, fourth-, alternative sixth-, and alternative eighth-order theories, however. This would mean that there is no benefit to use the higher-order theories to get the correct surface energy.

For the sixth- and eighth-order theories, the rate looks suboptimal. We discuss this issue further in Section 3.4 in the context of the coupled problem, but we do not know yet how we can solve it.

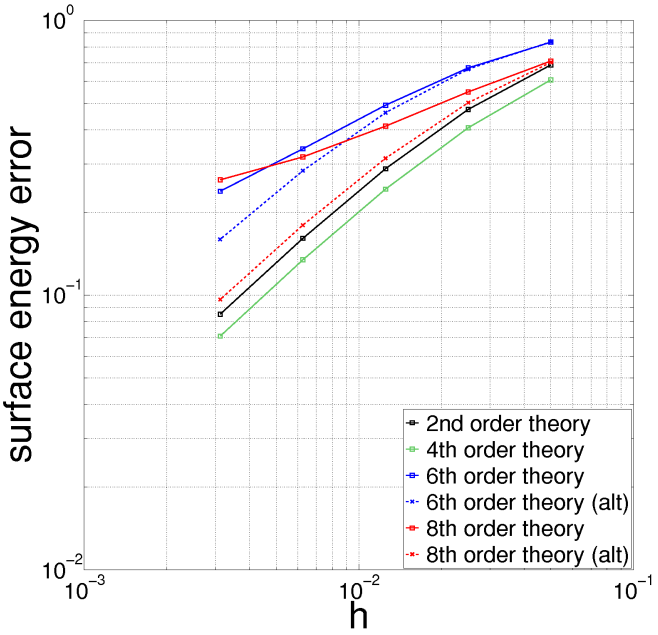

FIGURE 3.15. The surface energy errors are plotted against the mesh size.

3.3. Problem 3: Finding the Two Fields Together

Let us consider the coupled problem. We want to find the pair $\{u_h, c_h\}$ that solves the momentum equation and the phase field equation:

$$\begin{cases} -(c_h^2 E u_h')' = 0 \\ c_h E (u_h')^2 + G_c \delta c_h = 0 \end{cases} . \tag{3.18}$$

In order to reduce the computational cost, we alternatingly solve these two equations, fixing one field while solving for the other. We repeat this alternation multiple times to refine the solutions. The terms to solve for are highlighted in red above; in essence, we solve the momentum equation for the displacement field, and the phase field equation for the phase field. We refer to Section 3.5 for the pseudocode and implementation details.

In our experiment, we used 4000, 8000, 16000, 32000, 64000, and 128000 elements. While we had alternated between the two equations 15 times, our results show that we could have gotten by with fewer iterations for this problem (5 iterations).

Figures 3.16–3.21 show graphs of the displacement and phase fields for each theory. We see that all theories yield a displacement field that very accurately represents the analytical solution, even when we use only 4000 elements. This high fidelity is unlike what we saw in the decoupled setting (see Figures 3.1–3.6).

The phase fields for the second-, fourth-, alternative sixth-, and alternative eighth-order theories nail down their corresponding analytical solutions well, and do converge to them as we h-refine the mesh. It is interesting that the FE solution approaches the analytical solution "from below" in the coupled problem, whereas it did "from above" in the decoupled setting (see Figures 3.9–3.14).

The phase fields for the sixth- and eighth-order theories, however, "pass" the analytical solutions (shown in dotted line) as we h-refine the mesh. Like in the decoupled setting, the FE solutions are converging to a solution that is different from the analytical solution.

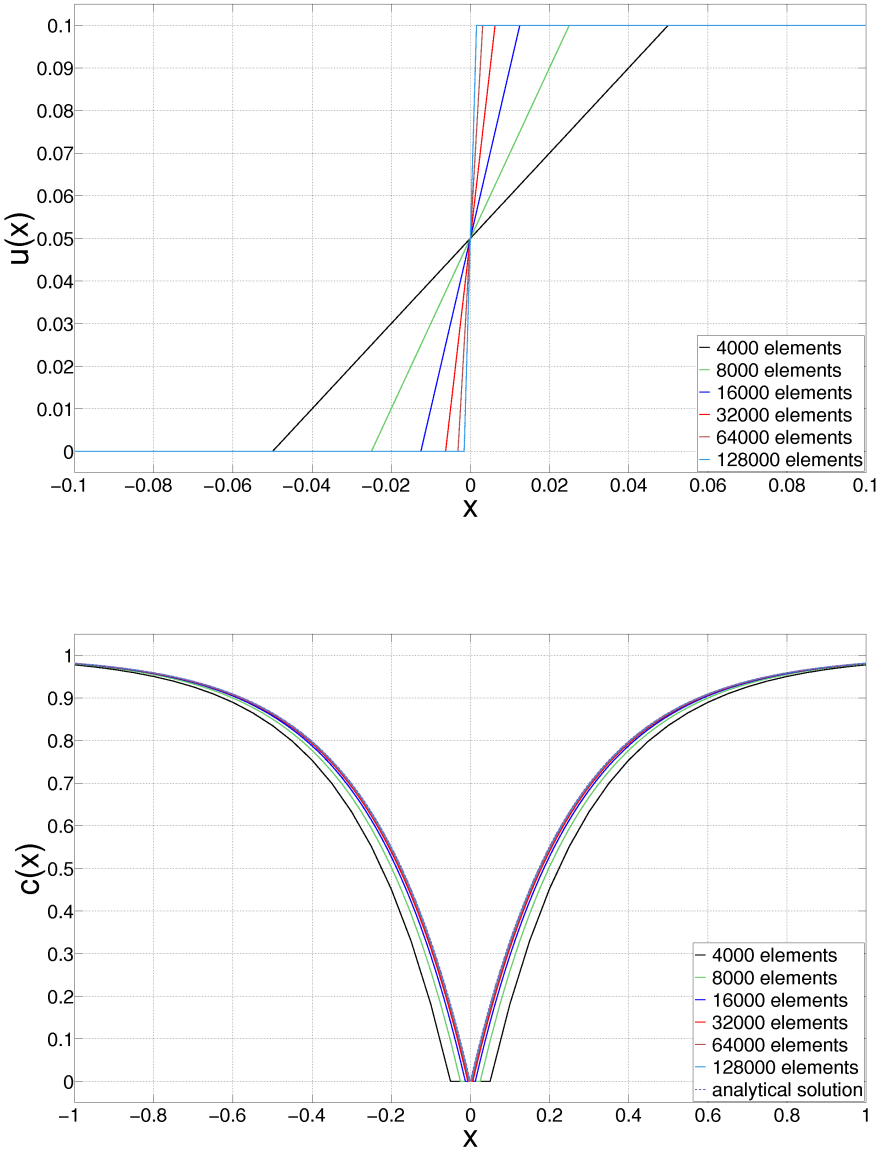

FIGURE 3.16. The displacement and phase fields from the second-order theory.

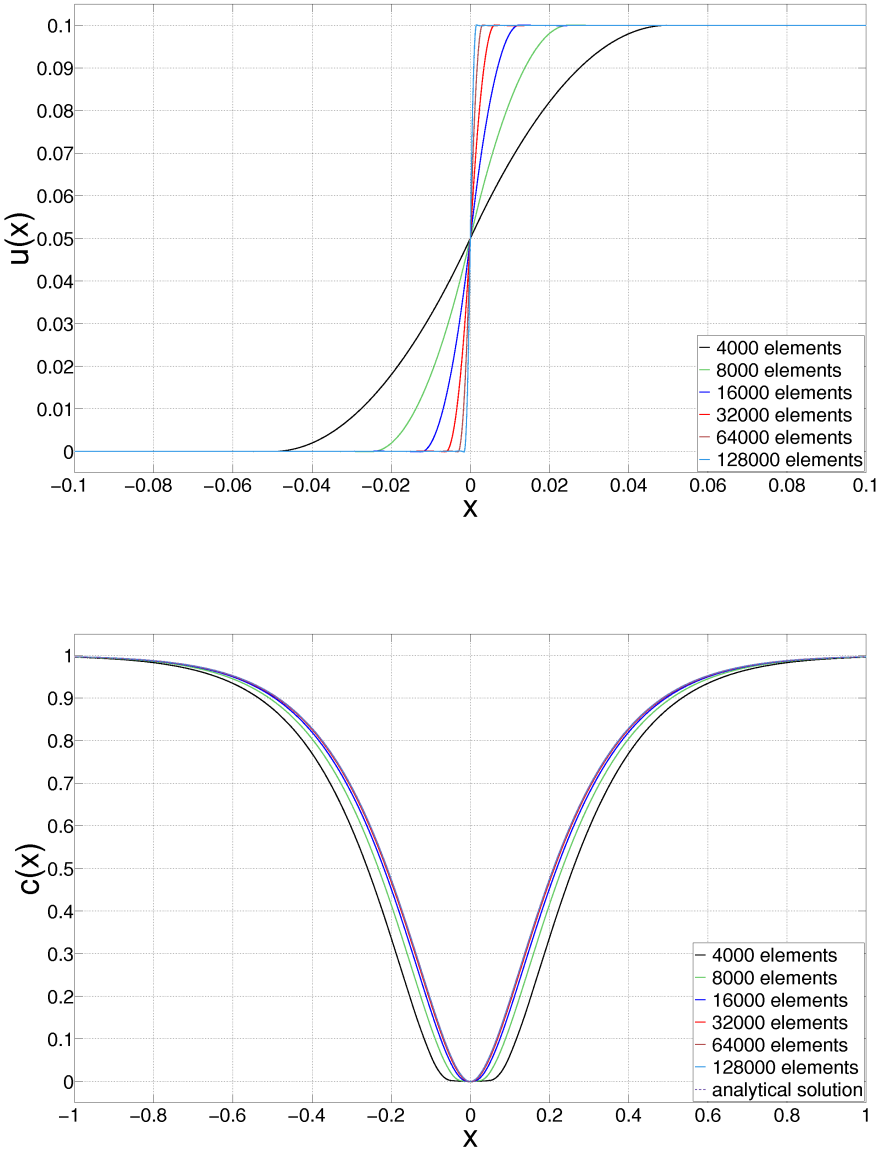

FIGURE 3.17. The displacement and phase fields from the fourth-order theory.

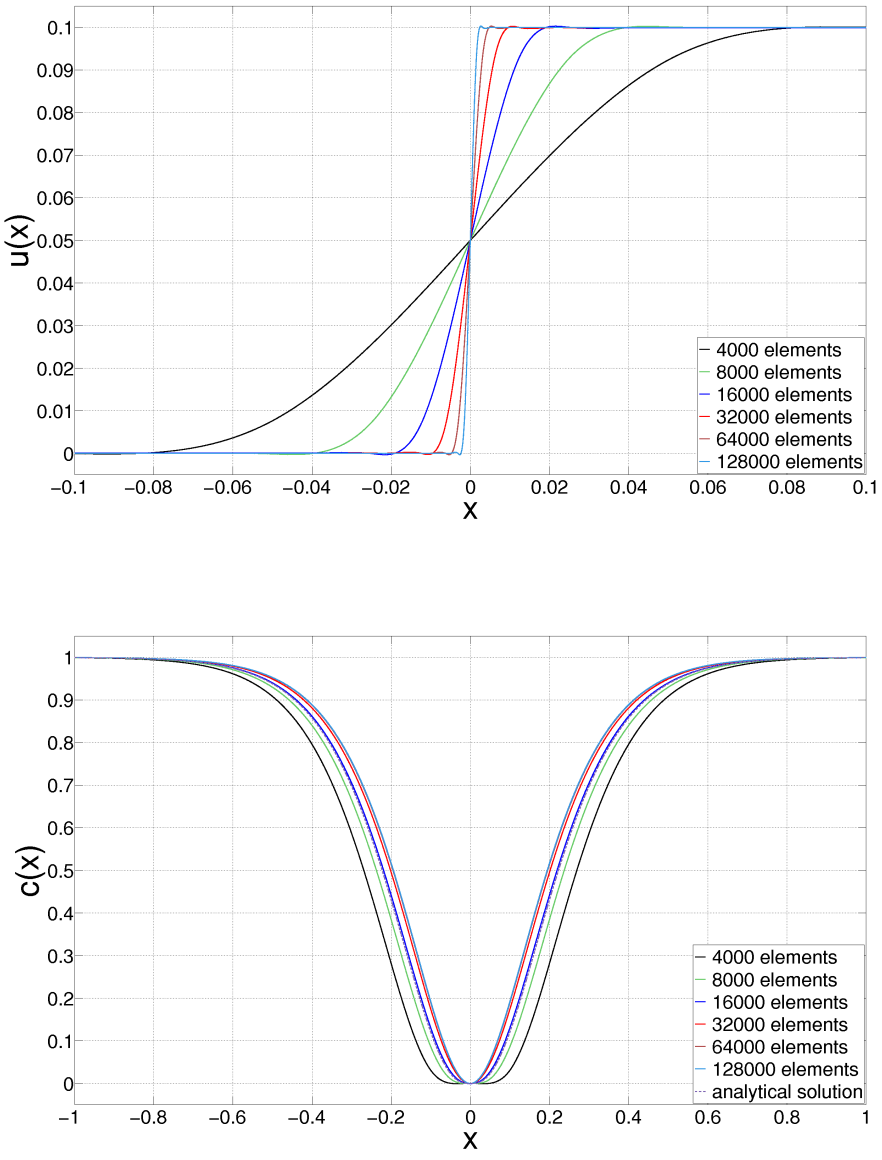

FIGURE 3.18. The displacement and phase fields from the sixth-order theory.

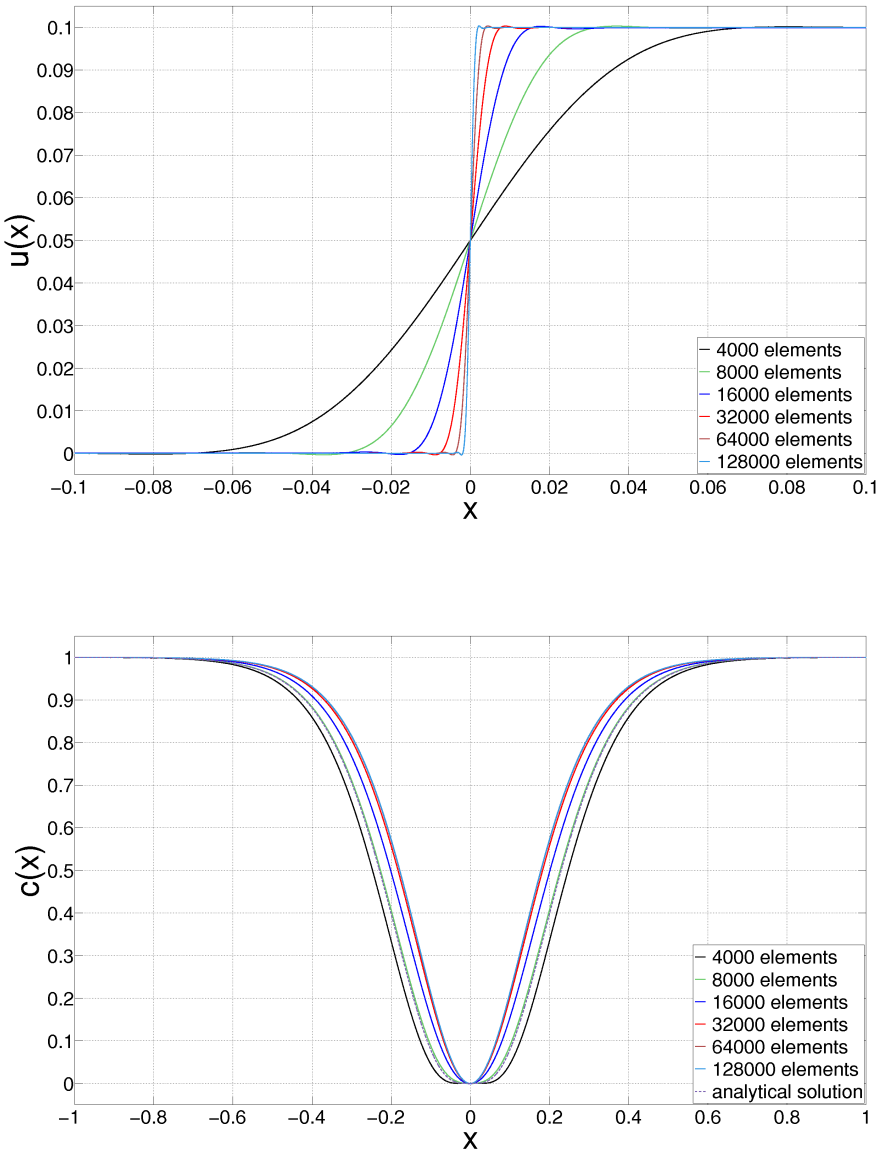

FIGURE 3.19. The displacement and phase fields from the eighth-order theory.

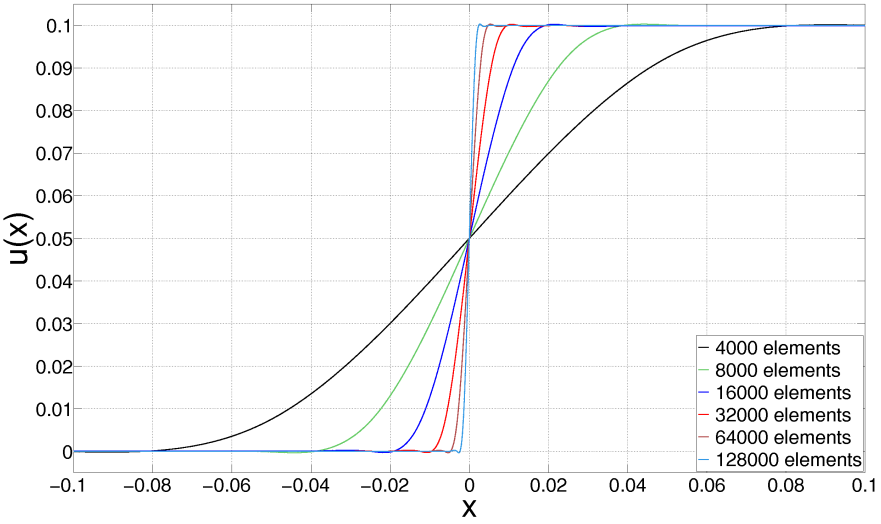

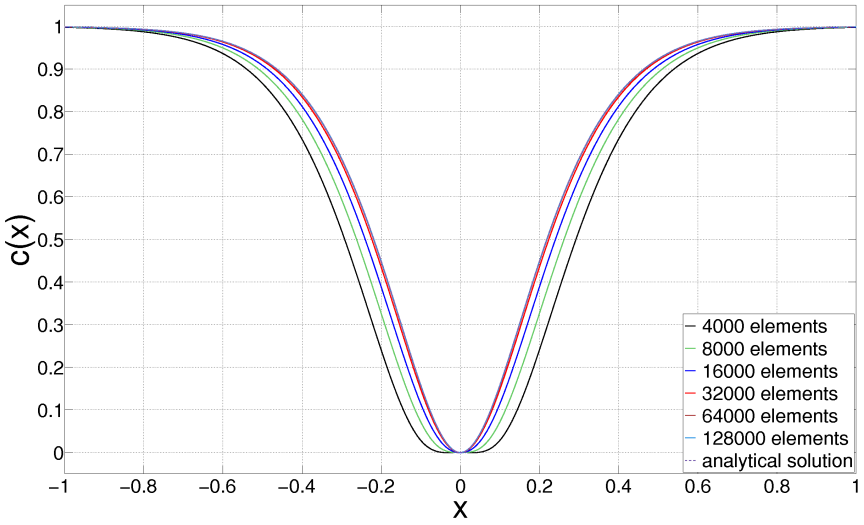

FIGURE 3.20. The displacement and phase fields from the alternative sixth-order theory.

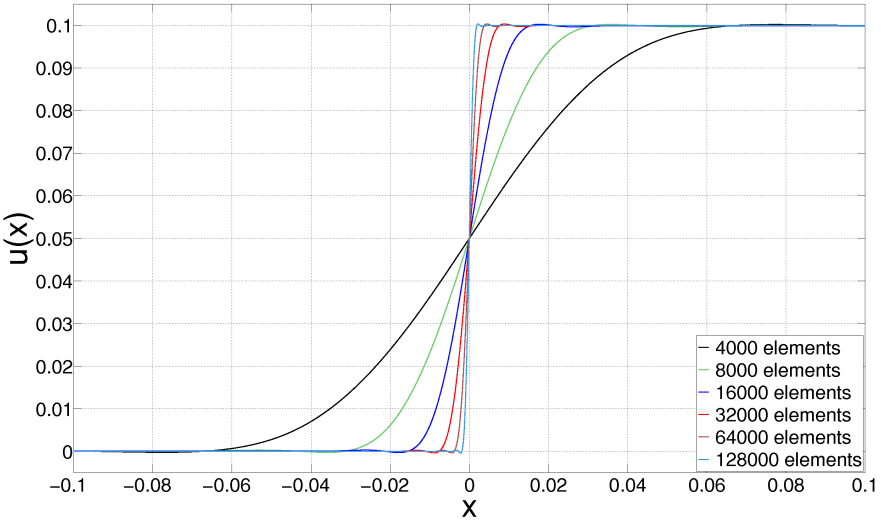

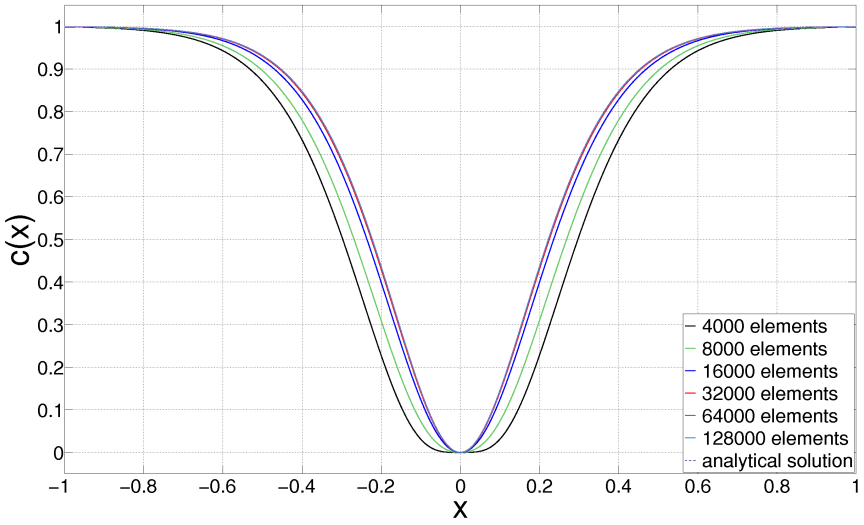

FIGURE 3.21. The displacement and phase fields from the alternative eighth-order theory.

Recall from (1.3) that our objective is to minimize the body's total potential energy. So to quantify how good the theories are, let us consider the error in the potential energy. Recall that,

$$\text{potential energy error} = \underbrace{\text{strain energy error}}_{(3.4)} + \underbrace{\text{surface energy error}}_{(3.17)}. \tag{3.19}$$

Figure 3.22 shows how the potential energy error behaves as we h-refine the mesh. We see that the error decreases to 0 for the second-, fourth-, alternative sixth-, and alternative eighth-order theories. The error for the fourth-order theory clearly converges faster than that for the second-order theory. The alternative sixth- and eighth-order theories seem to be unable to give even faster rate of convergence, however.

The potential energy errors for the sixth- and eighth-order theories decrease initially, but they increase soon after and plateau. The kink in the plots—around 8000 or 16000 elements—corresponds to the moment where the FE solution of the phase field "passed" the analytical solution. We would then expect the surface energy error to stop decreasing and start increasing as we refine the mesh. Figure 3.23 shows the individual contributions of the strain energy and surface energy errors. We see from the plot of the surface energy error that this is indeed the case.

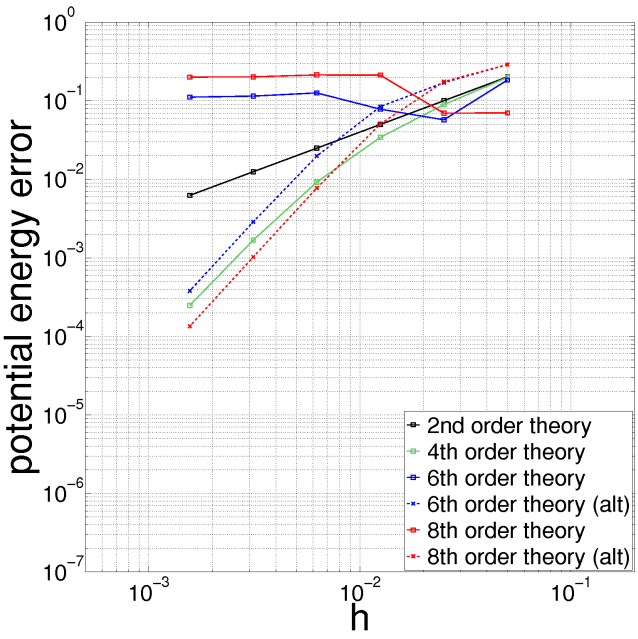

FIGURE 3.22. The potential energy error is plotted against the mesh size.

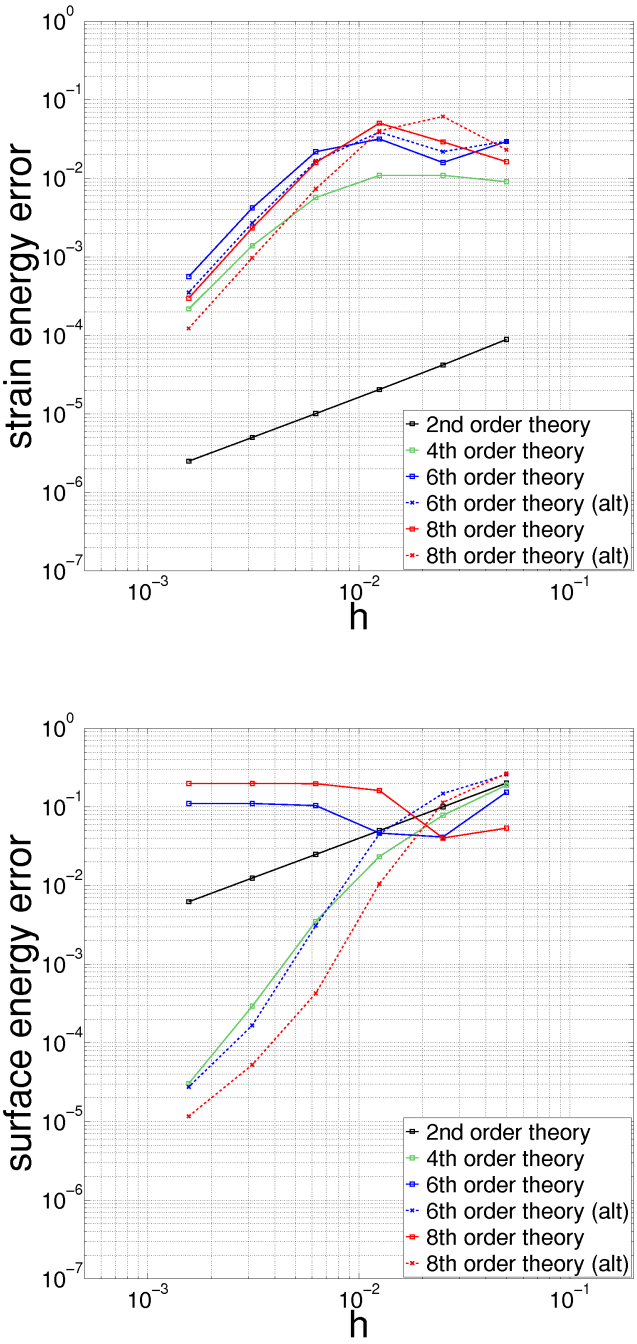

FIGURE 3.23. The strain energy and surface energy errors are plotted against the mesh size.

The table below lists the rates of convergence of the strain energy, the surface energy, and the potential energy errors. The errors for 32000, 64000, and 128000 elements were used to calculate the slope of the least-squares line.

We see that, indeed, the fourth-order theory works and allows a faster convergence when compared to what the second-order theory can do. (The strain energy error is much smaller for the second-order theory for the mesh sizes that we considered.) However, it is not clear what the theoretical rates of convergence should be for the fourth-order theory.

The strain and potential energies converge a bit faster if we use the alternative sixth- and eighth-order theories. However, we make this claim with reservation for two reasons. From the plot of the strain energy error, we see that the error for the fourth-order theory has not quite landed in the asymptotic range with 32000 elements. Furthermore, we see a stagnation in convergence in the plot of the surface energy error, possibly due to some numerical errors. The few data points in the middle shows some promise that we could actually get a higher rate of convergence, but we have not attempted to verify this.

theory	rate of convergence		
	strain	surface	potential
2nd-order	1.007	1.001	1.001
4th-order	2.355	3.425	2.608
6th-order	2.641	–0.044	0.089
8th-order	2.869	–0.006	0.048
alternative 6th-order	2.784	3.406	2.852
alternative 8th-order	2.952	2.599	2.927

3.4. Degeneration of Phase Field in the Sixth- and Eighth-Order Theories

For both the decoupled and the coupled problems, we saw that the phase fields for the sixth- and eighth-order theories were not converging to the analytical solutions (2.6) and (??). The problem is that the Neumann BCs that we imposed upon the FE solution do not represent all of the continuity conditions that we had specified for the analytical solution. Below, we illustrate this for the coupled problem.

Let us plot the derivatives of c_h for the sixth-order theory (shown in Figure 3.24). Recall that we had specified $c(0)$, $c'(0)$, $c''(0)$ to be zero at the crack. However, what we see at $x = 0$ is that the second derivative of c_h does not converge to 0 as we let $h \to 0^+$. Interestingly, the (jump in) third derivative of c_h does converge to 0 at $x = 0$.

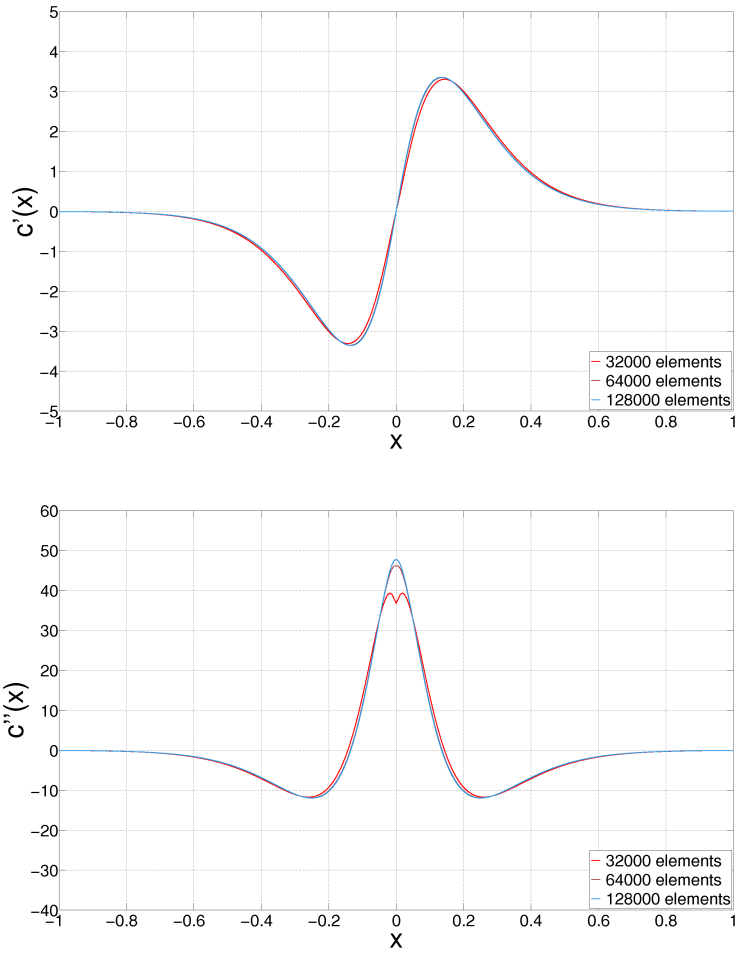

FIGURE 3.24. Derivatives of the phase field for the sixth-order theory. We see that $c_h''(0) \not\to 0$, but $c_h'(0)$, $c_h'''(0) \to 0$.

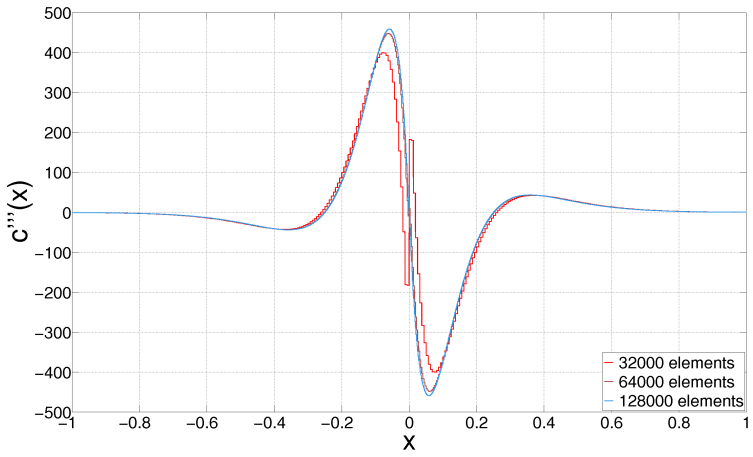

FIGURE 3.24. Derivatives of the phase field for the sixth-order theory. We see that $c_h''(0) \not\to 0$, but $c_h'(0)$, $c_h'''(0) \to 0$.

What about the eighth-order theory, where we had let $c(0)$, $c'(0)$, $c''(0)$, $c'''(0) = 0$? Figure 3.25 shows that the second derivative and the (jump in) fourth derivative of c_h do not converge to 0 at $x = 0$, but the third and fifth derivatives do. (The fifth derivative, for quartic B-splines, will have Dirac deltas at the element interfaces. But for brevity, we will assume it to be identically zero and do not show it below.)

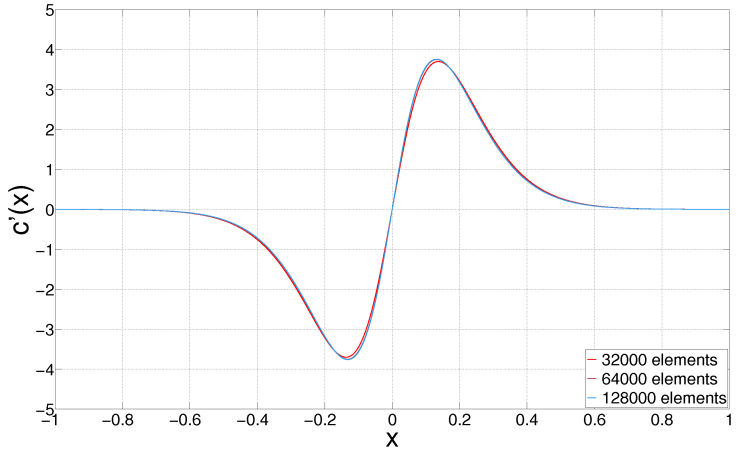

FIGURE 3.25. Derivatives of the phase field for the eighth-order theory. We see that $c_h''(0)$, $c_h^{(4)}(0) \not\to 0$, but $c_h'(0)$, $c_h'''(0)$, $c_h^{(5)}(0) \to 0$.

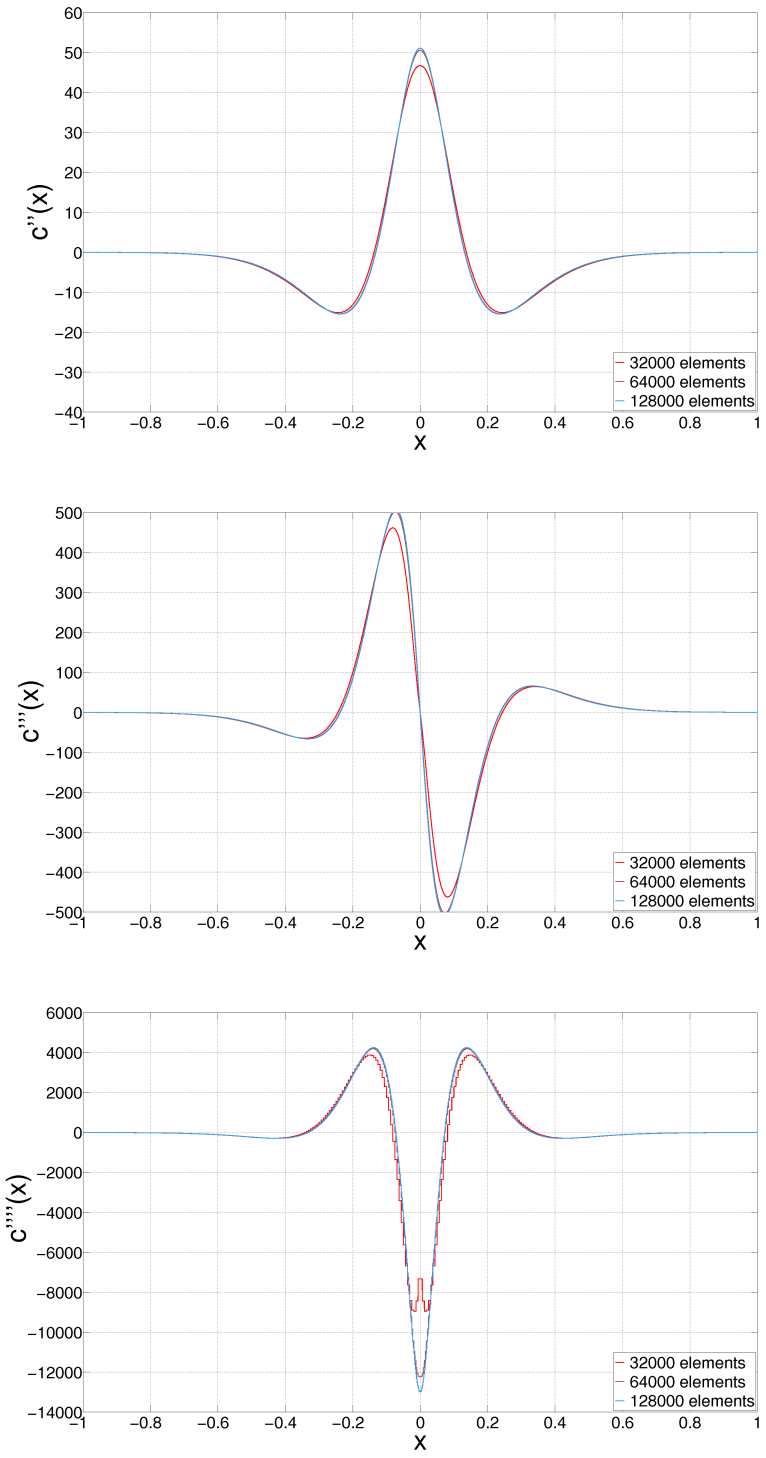

FIGURE 3.25. Derivatives of the phase field for the eighth-order theory. We see that $c_h''(0)$, $c_h^{(4)}(0) \not\to 0$, but $c_h'(0)$, $c_h'''(0)$, $c_h^{(5)}(0) \to 0$.

It is as though the FE solutions of the phase field for the sixth- and eighth-order theories are converging to analytical solutions given by their alternative counterparts. To test this claim, we graph a family of analytical solutions, which are of the forms (2.7) and (??), by varying k from 1 to 2 in increment of 1/8. Then, we overlay the graph of the FE solution for 128000 elements to see if it matches any of the analytical solutions.

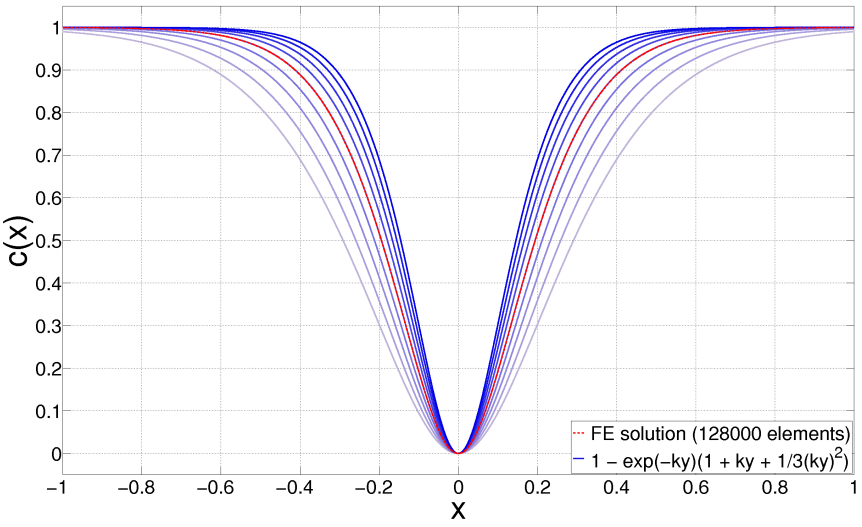

FIGURE 3.26. The FE solution of the sixth-order theory matches the analytical solution of the alternative sixth-order theory that we would have obtained with $k = 3/2$.

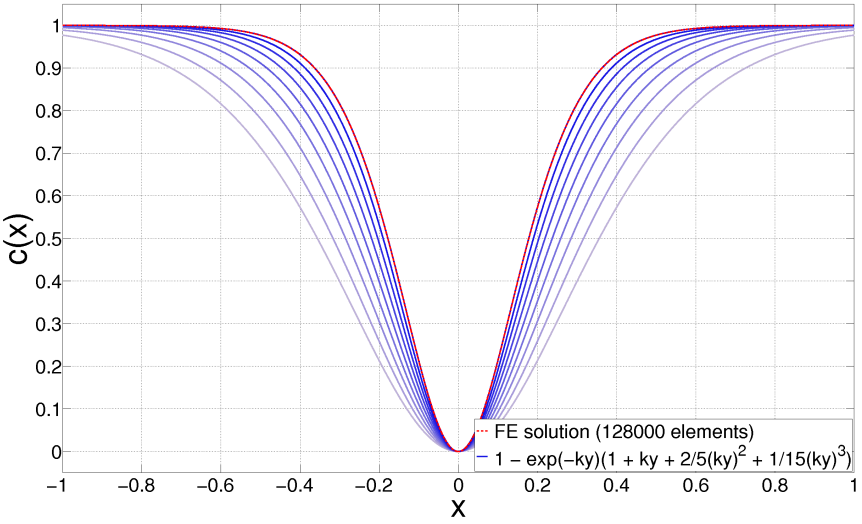

FIGURE 3.27. The FE solution of the eighth-order theory matches the analytical solution of the alternative eighth-order theory that we would have obtained with $k = 2$.

Figures 3.26 and 3.27 show that the FE solutions of the phase field for the sixth- and eighth-order theories do match the analytical solutions of their alternative counterparts. In other words, we had been solving the problem using the alternative sixth- and eighth-order theories all along.

Note that the alternative theories are not the ones we had before with $k = 4/3$ and $k = 8/5$. Instead, we have $k = 3/2$ and $k = 2$. The normalization in 1D still holds, so the change in k means that the phase field's length scale ℓ_0 has been changed.

Perhaps this should not come as a surprise. Recall from Section 2 that both versions of the sixth-order theories involved the same EL equation (2.2) with the same coefficients $\{a_1, a_2, a_3\}$ in terms of k (similarly with the eighth-order theories). The only thing that differentiated the two versions were the continuity conditions, which are only partially embedded in our natural BCs.

Currently, we do not have a rigorous explanation for why the natural BCs can fully capture the continuity conditions for the second-, fourth-, alternative sixth-, and alternative eighth-order theories, whereas they cannot for the sixth- and eighth-order theories. We will need to examine how the sixth- and eighth-order differential operators behave in the weak form, and if there are problems inherent in these operators that we had not taken care of.

3.5. Appendix for Chapter 3

Here, we outline our code for the coupled problem. Since dynamics is absent (so far), we treat the iteration count for alternation as "time." So let $\vec{u}^{(t)}$ and $\vec{c}^{(t)}$ represent the vectors of coefficients for u_h and c_h at time $t = 0, 1, 2, \cdots$.

// **Initialize**

· Set the model parameters.

· Create an open, uniform knot vector with appropriate degree.

· Set the Gaussian quadrature rule (8-point).

· Set the final time t_{final}, i.e. specify how many times we will alternate between the two equations.

· Make an initial guess for the phase field $\vec{c}^{(0)}$. To be impartial to all the theories, we always take $\vec{c}^{(0)}$ to be the L^2-projection of

$$\tilde{c}(x) = \begin{cases} 1, & \text{if } |x| > 2\ell_0 \\ 0, & \text{if } |x| \leq 2\ell_0 \end{cases}$$

onto the B-spline basis functions.

// **Begin marching in time**

For $t = 1, 2, \cdots, t_{\text{final}}$, do the following:

1. Solve the momentum equation for $\vec{u}^{(t)}$.

· Use the phase field $\vec{c}^{(t-1)}$ from the previous time to form the stiffness matrix K and the RHS vector $\vec{f}\,(= \vec{0})$.

· Use the Dirichlet BCs to reduce the system. Now, $K \in \mathbb{R}^{(n-2)\times(n-2)}$ and $\vec{f}\,(\neq \vec{0}) \in \mathbb{R}^{n-2}$.

· Solve the equation $K\vec{u} = \vec{f}$ for the displacement $\vec{u}$.

· Set $\vec{u}^{(t)} = \vec{u}$.

2. Solve the phase field equation for $\vec{c}^{(t)}$.

· Make an initial guess $\vec{c}^{(t)}_{\text{guess}}$ for the Newton's method. For the first Newton's step, we use $\vec{c}^{(t-1)}$ from the previous time. In later steps, we use the updated value $\vec{c}^{(t)}_{\text{guess}}$ from the previous step.

· Use the displacement $\vec{u}^{(t)}$ from the current time to form the consistent tangent matrix K and the RHS vector $\vec{f}$, which represents the current residual.

· Solve the equation $K(\Delta\vec{c}) = \vec{f}$ for the Newton's increment $\Delta\vec{c}$.

· Update the guess, i.e. $\vec{c}^{(t)}_{\text{guess}} \leftarrow \vec{c}^{(t)}_{\text{guess}} + \Delta\vec{c}$.

· Terminate the Newton's method if we reach convergence or the maximum number of iterations. Set $\vec{c}^{(t)} = \vec{c}^{(t)}_{\text{guess}}$.

Because we may want to consider degradation functions other than $g(c) = c^2$, we had implemented Newton's method to iteratively solve the phase field equation. In addition, once we had solved a matrix equation (resulting from the weak form of either equation), we would apply iterative refinement to ensure that our solution is accurate. To evaluate integrals over an element, we used the 8-point Gaussian quadrature for all the theories.

In our numerical simulation, we terminated the loops in these manners:

loop	termination criterion
physics (the two equations)	unconditionally after 15 iterations
Newton's method	1 iteration min., 5 iterations max., terminate in-between if the 2-norm of the residual vector is below 10^{-14}
iterative refinement	10^3 iterations min., 10^4 iterations max., terminate in-between if the ∞-norm of the residual vector is below 10^{-14}

4. Conclusion

Based on the existing second- and fourth-order phase field theories, we considered a sharp interface problem in 1D to develop the higher-order theories. By imposing a set of continuity conditions for the analytical solution of the phase field, we were able to come up with two sixth-order and two eighth-order theories.

Our numerical results show that, for the type of natural BCs that we imposed on the phase field, the alternative sixth- and alternative eighth-order theories are the right models to work with, in the sense that the FE solutions of the displacement and phase fields did converge to the analytical solutions. However, we know that, when compared to the fourth-order theory, we cannot achieve a faster convergence in the errors if we use the alternative sixth- and alternative eighth-order theories.

We will need to further study the phase field models from a mathematical aspect, so that we may find the higher-order theories that (1) give the right solutions and (2) result in a fast convergence of errors. The second point may be guaranteed by the sixth- and eighth-order theories that we developed here, in which case we would just need to find the right set of BCs for the phase field to fully capture the continuity conditions.

In addition, the Gamma convergence of the approximate potential energy has yet to be established for the fourth-order theory and the higher-order theories. Even for the second-order theory, it has been shown for only simple cases. We hope to consider this problem one day.

Acknowledgment

I want to thank Mike and Tom for providing me the chance to work on this project with them and helping me find my way into research. I wish Mike and his family all the best as they move to North Carolina. I also want to thank Dr. Chad Landis for his advice on how to approach the phase field theories.

References

[1] M. J. Borden, T. J. R. Hughes, C. M. Landis, and C. V. Verhoosel, "A Higher-Order Phase-Field Model for Brittle Fracture: Formulation and Analysis Within the Isogeometric Analysis Framework", *ICES Report 13-20*, (2013).

[2] B. Bourdin, G. A. Francfort, and J.-J. Marigo, "Numerical Experiments in Revisited Brittle Fracture", *Journal of the Mechanics and Physics of Solids*, (2000).

[3] G. A. Francfort and J.-J. Marigo, "Revisiting Brittle Fracture as an Energy Minimization Problem", *Journal of the Mechanics and Physics of Solids*, (1998).

[4] C. Miehe, M. Hofacker, and F. Welschinger, "A Phase Field Model for Rate- Independent Crack Propagation: Robust Algorithmic Implementation Based on Operator Splits", *Computer Methods in Applied Mechanics and Engineering*, (2010).

5. Revisiting Higher-Order Theories

The momentum and phase field equations, when we had decoupled them and solved them alternatingly, led us to incorrect solutions for the sixth- and eighth-order theories. We reasoned that this is because, when we derive the Euler-Lagrange equations from the potential energy functional, we do not explicitly impose the derivatives of the phase field to equal to 0 at a crack.

5.1. Motivation for the use of Lagrange multipliers

In optimization, constraints are enforced by Lagrange multipliers. A classic example of a constraint in mechanics is incompressibility of a material. Here, as an illustration, we consider minimizing the potential energy $\tilde{\Psi} = \tilde{\Psi}(u,\, c)$ for the 1D bar in tension using the sixth-order theory. The following analysis applies to both the analytical solutions and the FE solutions, so u and c can denote either set of fields.

Recall that, in order for the error in the strain energy to diminish rapidly, the 0th, 1st, and 2nd derivatives of the phase field must equal to 0 at a crack. In other words, we have three constraints to satisfy:

$$c(x) = 0, \;\; c'(x) = 0, \;\; c''(x) = 0, \;\; \text{for all } x \in \Gamma.$$

We have a dilemma. These equations hold true for all points in Γ, the cracked surface, but we do not know what Γ is. After all, we are trying to represent Γ using the phase field. So the constraints above suffer from a circular logic. We could instead write down a statement such as "For any point $x \in \Omega$, if $c(x) = 0$, then $c''(x) = 0$." in an average or a weak sense, i.e.

$$\int_\Omega (1 - c)\, c''\; dx = 0.$$

However, the analytical solution of the phase field does not even satisfy this equation, so we cannot expect the FE solution to either.

In order to find the right constraints, let us re-examine the expression of the potential energy for the second-order theory. There, we did not impose the constraint $c(x) = 0$ for $x \in \Gamma$, but somehow, we ended up satisfying them. There must be something to the potential energy functional. Recall that, for the 1D problem of a bar in tension,

$$\tilde{\Psi}(u,\, c) = \int_\Omega c^2\, \frac{E}{2}(u')^2\; dx + \int_\Omega \frac{G_c}{4\ell_0}\Big[(1-c)^2 + 4\ell_0^2 (c')^2\Big]\; dx.$$

We believe that, by alternatingly minimizing the potential energy, the strain energy term corrects what the displacement field should look like given a phase field, and vice versa. In particular, if the displacement field is supposed to be discontinuous at $x \in \Omega$, then the derivative term $(u'(x))^2$ would be large, which forces the phase field to be small around a neighborhood of x so that the energy can reach a local minimum.

In other words, to some extent, we had been using the Lagrange multiplier method all along. Unlike in an actual Lagrange multiplier method, where the Lagrange multiplier field $\lambda = \lambda(x)$ can grow and change over iterations, the Lagrange multiplier here is kept a constant function of $\lambda(x) = 1$ throughout all iterations.

What about the fourth-order theory? The fact that we obtained $c_h(0) \approx 0$ in our numerical simulations can be explained by the above, but not $c_h'(0) \approx 0$. We argue that this was a coincidence that resulted from the shape of the phase field about the crack. Since the phase field is C^1 in the fourth-order theory, the derivative of the phase field must intersect 0 as it continuously transitions from a negative to positive value.

We propose that, for all theories, Lagrange multipliers should be used in order to correctly minimize the potential energy and to correctly satisfy the derivative constraints for the phase field. In particular, we advocate the use of augmented Lagrangian method, which combines the Lagrange multiplier method and the quadratic penalty method for better conditioning of the tangent matrix.

5.2. Augmented Lagrangian method

5.2.1. Notations

To write down the new objective function using the augmented Lagrangian method, let us first introduce some notations. Let $g = g(u, c)$ denote a constraint, and $\lambda = \lambda(x)$ the corresponding Lagrange multiplier. In particular, we will add an index to g and λ as a subscript to indicate the order of the derivative of c in the constraint. The particular constraints that we will use are,

$$\begin{aligned} g_0(u, c) &= c^2 \frac{E}{2}(u')^2, \\ g_1(u, c) &= \ell_0^2 (c')^2 \frac{E}{2}(u')^2, \\ g_2(u, c) &= \ell_0^4 (c'')^2 \frac{E}{2}(u')^2, \\ g_3(u, c) &= \ell_0^6 (c''')^2 \frac{E}{2}(u')^2. \end{aligned} \tag{5.1}$$

Clearly, these are motivated by our analysis of the second-order theory. For consistency, we inserted a constant, power of ℓ_0 to g_1, g_2, and g_3, so that the resulting expressions have the dimension of energy. Note that we only use the constraints that are needed by a particular theory. For example, for the sixth-order theory, we only use g_0, g_1, and g_2.

Corresponding to these constraints, we have the Lagrange multipliers:

$$\begin{aligned} \lambda_0 &= \lambda_0(x), \\ \lambda_1 &= \lambda_1(x), \\ \lambda_2 &= \lambda_2(x), \\ \lambda_3 &= \lambda_3(x). \end{aligned} \tag{5.2}$$

Since we are dealing with a minimization problem and the constraints g are nonnegative by design, we assume that the Lagrange multipliers λ are nonnegative everywhere. In particular, the Lagrange multipliers must be nonnegative at initialization. Unlike the displacement and phase fields, we do not expand λ as a linear combination of B-splines. We will soon see that we just need to keep track of the value of λ at the quadrature points. These values will be updated at each iteration through a post-process calculation. Again, we only use Lagrange multipliers that are needed for a particular theory.

Finally, we remark that we will enforce the constraints using the Lagrange multipliers weakly, i.e. we require that

$$\begin{aligned}
\int_\Omega \lambda_0\, g_0\; dx &= 0,\\
\int_\Omega \lambda_1\, g_1\; dx &= 0,\\
\int_\Omega \lambda_2\, g_2\; dx &= 0,\\
\int_\Omega \lambda_3\, g_3\; dx &= 0.
\end{aligned} \tag{5.3}$$

These equations hold true for the analytical solutions, so we can expect the FE solutions to satisfy them well.

5.2.2. Expression for the Objective Function

For the Lagrange multiplier method, we just need to append the constraints (**??**) to the potential energy to obtain the new objective function (which we still denote by $\tilde{\Psi}$). For the sixth-order theory, we get

$$\tilde{\Psi}(u,\, c,\, \lambda) = \int_\Omega c^2\, \frac{E}{2}(u')^2\; dx + \int_\Omega G_c \Gamma_{c,6}\; dx + \int_\Omega \left(\lambda_0\, g_0 + \lambda_1\, g_1 + \lambda_2\, g_2\right)\; dx,$$

and we would minimize $\tilde{\Psi}$ over a larger space $(u,\, c,\, \lambda) \equiv (u,\, c,\, \lambda_0,\, \lambda_1,\, \lambda_2)$. Note that when we take the variational derivative of $\tilde{\Psi}$ over a Lagrange multiplier λ, we get the corresponding the constraint g back.

For the quadratic penalty method, we append the square of the constraints g^2 to the potential energy. The square terms are penalized by a constant $\beta > 0$. In other words, the new objective function for the sixth-order theory is,

$$\tilde{\Psi}(u,\, c) = \int_\Omega c^2\, \frac{E}{2}(u')^2\; dx + \int_\Omega G_c \Gamma_{c,6}\; dx + \beta \int_\Omega \left(g_0^2 + g_1^2 + g_2^2\right)\; dx.$$

The penalization constant β must approach infinity in order for us to really solve the original constrained problem. We can multiply β by 10 after each iteration, for example, but as β becomes large, the tangent matrix may become ill-conditioned.

The augmented Lagrangian method combines the two methods above. We seek to minimize the following objective function:

$$\boxed{\begin{aligned}
\tilde{\Psi}(u,\, c,\, \lambda) = &\int_\Omega c^2\, \frac{E}{2}(u')^2\; dx + \int_\Omega G_c \Gamma_{c,6}\; dx\\
&+ \int_\Omega \left(\lambda_0\, g_0 + \lambda_1\, g_1 + \lambda_2\, g_2\right)\; dx + \beta \int_\Omega \left(g_0^2 + g_1^2 + g_2^2\right)\; dx.
\end{aligned}} \tag{5.4}$$

We can show that, unlike in the quadratic penalty method, we do not need to increase β indefinitely in order to achieve convergence in the iterative scheme that we will describe next. Ill-conditioning is therefore less of a problem, and the choice of initial guess less critical (see Nocedal and Wright's "Numerical Optimization").

Energies computed after 15 iterations.

Before: only the Dirichlet BCs are satisfied for the phase field

theory	energy	number of elements					
		4000	8000	16000	32000	64000	128000
2nd-order	strain	8.892e−5	4.206e−5	2.048e−5	1.011e−5	5.022e−6	2.503e−6
	surface	1.201487	1.100332	1.050063	1.025006	1.012496	1.006247
	potential	1.201576	1.100374	1.050084	1.025016	1.012501	1.006249
4th-order	strain	9.070e−3	1.092e−2	1.089e−2	5.702e−3	1.388e−3	2.179e−4
	surface	1.189696	1.078644	1.023418	1.003532	1.000294	1.000031
	potential	1.198766	1.089566	1.034305	1.009234	1.001681	1.000248
6th-order	strain	2.943e−2	1.589e−2	3.176e−2	2.180e−2	4.193e−3	5.607e−4
	surface	1.154540	1.041568	0.953359	0.895549	0.889172	0.888922
	potential	1.183968	1.057462	0.985117	0.917354	0.893366	0.889483
8th-order	strain	1.630e−2	2.915e−2	5.044e−2	1.592e−2	2.336e−3	2.986e−4
	surface	1.053986	0.959589	0.837756	0.801755	0.800090	0.800016
	potential	1.070291	0.988736	0.888198	0.817680	0.802426	0.800314

Energies computed after 15 iterations.

Now: both the Dirichlet BCs and the continuity conditions are satisfied for the phase field

theory	energy	number of elements					
		4000	8000	16000	32000	64000	128000
2nd-order	strain	3.238e−17	1.462e−17	6.972e−18	3.408e−18	1.685e−18	8.379e−19
	surface	1.354715	1.254701	1.204701	1.179701	1.167201	1.160951
	potential	1.354715	1.254701	1.204701	1.179701	1.167201	1.160951
4th-order	strain	1.710e−17	6.796e−18	3.028e−18	1.428e−18	6.942e−19	3.445e−19
	surface	1.231752	1.125850	1.074370	1.049000	1.036407	1.030134
	potential	1.231752	1.125850	1.074370	1.049000	1.036407	1.030134
6th-order	strain	5.266e−17	1.894e−17	7.910e−18	3.598e−18	1.716e−18	8.449e−19
	surface	1.420449	1.205145	1.101288	1.050322	1.025081	1.012520
	potential	1.420449	1.205145	1.101288	1.050322	1.025081	1.012520
8th-order	strain	4.316e−17	1.526e−17	6.339e−18	2.879e−18	1.372e−18	6.718e−19
	surface	1.438140	1.209649	1.102419	1.050605	1.025151	1.012538
	potential	1.438140	1.209649	1.102419	1.050605	1.025151	1.012538

5.2.3. Second attempt

This time, we focus on the 6th-order theory and consider what we can do differently to the phase field equation. After all, we need to fix the phase field solution, and this is obtained from the phase field equation. We can consider the following choices:

$$F(\vec{\chi}) = \int_\Omega (1-c_h)^2 \, dx, \quad \int_\Omega (c_h')^2 \, dx, \quad \int_\Omega (c_h'')^2 \, dx, \quad \int_\Omega (c_h''')^2 \, dx.$$

It turns out $(c_h'')^2$ is the right choice. This may be obvious in retrospect, as we are, in some sense, penalizing the phase field if its second derivative is nonzero at a point. Note that the first choice will lead to a discernible overshoot in the phase field near the crack, and a slowly linearly-growing displacement field (similar to the one in Figure 3.1). The second choice does give us FE solutions that are close to the analytical solutions; however, we still do not get $c_h''(0) \to 0$ as we refine the mesh. The last choice seems to be the worst, as Newton's method diverges after each iteration and we soon encounter a singular tangent matrix.

We scale F so that it matches the existing expression for the crack density functional $\Gamma_{c,6}$, and so that the constant k is dimensionless:

$$\boxed{F(\vec{\chi}) = \int_\Omega \frac{G_c}{4\ell_0} \cdot \ell_0^4 (c_h'')^2 \, dx}. \tag{5.5}$$

In other words, for the 6th-order theory,

$$\tilde{\Psi}_{convex}(\vec{\chi}) = \left(\int_\Omega g(c_h) \cdot \frac{1}{2} E (u_h')^2 \, dx + \int_\Omega G_c \Gamma_{c_h,6} \, dx \right) + k \int_\Omega \frac{G_c}{4\ell_0} \cdot \ell_0^4 (c_h'')^2 \, dx,$$

$$\tilde{\Psi}_{concave}(\vec{\chi}) = -k \int_\Omega \frac{G_c}{4\ell_0} \cdot \ell_0^4 (c_h'')^2 \, dx.$$

This time, F does not depend on the displacement field, so we only need to change the phase field equation. In particular, Newton's method results in,

$$\begin{aligned} K_{AB} = &\left(g''(c_h) \cdot \frac{1}{2} E (u_h')^2 \, N_B, \, N_A \right) \\ &+ \frac{G_c}{2\ell_0} \left[(N_B, \, N_A) + \frac{4\ell_0^2}{3} (N_B', \, N_A') + \frac{16\ell_0^4}{27} (N_B'', \, N_A'') + \frac{64\ell_0^6}{729} (N_B''', \, N_A''') \right] \\ &+ k \left[\frac{G_c}{2\ell_0} \cdot \ell_0^4 (N_B'', \, N_A'') \right], \end{aligned}$$

and

$$\begin{aligned} \vec{f}_A = &\left(g'(c_h) \cdot \frac{1}{2} E (u_h')^2, \, N_A \right) \\ &+ \frac{G_c}{2\ell_0} \left[(c_h, \, N_A) + \frac{4\ell_0^2}{3} (c_h', \, N_A') + \frac{16\ell_0^4}{27} (c_h'', \, N_A'') + \frac{64\ell_0^6}{729} (c_h''', \, N_A''') \right] \\ &+ k \left[\frac{G_c}{2\ell_0} \cdot \ell_0^4 (c_h'', \, N_A'') - \frac{G_c}{2\ell_0} \cdot \ell_0^4 (c_{h,old}'', \, N_A'') \right]. \end{aligned}$$

Note that $c_{h,old}$ is the solution from the previous CCCP iteration, and c_h is the current Newton's guess to the next CCCP iterate. Again, we only need to add a few terms (these are highlighted in red) to our existing code.

Recall that we had also run into the problem of $c_h''(0) \not\to 0$ for the 8th-order theory. Hence, let us also investigate what happens when we apply CCCP with (5.5) as F to the 8th-order theory.

Figures 5.1 and 5.2 show the displacement and phase fields that we get with $k = 10^6$. The displacement field for the 6th-order theory is not great initially, but soon becomes better as we refine the mesh. We can even plot the field for $x \in [-0.1, 0.1]$ again.

What is more remarkable is the phase field. Even with 4000 elements, the FE solution matches the analytical solution very well. Furthermore, from Figures 5.3 and 5.4, we see that the second derivative of the phase field does converge to 0 as we h-refine the mesh. Thus, we believe that (5.5) is the right choice to make.

What about the energies? Do they converge and how fast do they? We compute the strain, surface, and potential energies for the 6th- and 8th-order theories with CCCP. For reference, we list the energies for the 2nd- and 4th-order theories that we had gotten by alternatingly solving the equations (no CCCP). Recall that we should have a strain energy of 0, a surface energy of 1, and a potential energy of 1.

theory	energy	number of elements				
		4000	8000	16000	32000	64000
2nd-order	strain	0.000089	0.000042	0.000020	0.000010	0.000005
	surface	1.201487	1.100332	1.050063	1.025006	1.012496
	potential	1.201576	1.100374	1.050084	1.025016	1.012501
4th-order	strain	0.009070	0.010922	0.010888	0.005701	0.001388
	surface	1.189696	1.078644	1.023418	1.003532	1.000294
	potential	1.198766	1.089566	1.034305	1.009234	1.001681
6th-order	strain	2.839453	0.168893	0.007016	0.000256	0.000010
	surface	0.987284	0.993663	0.997961	0.999391	0.999760
	potential	3.826736	1.162556	1.004977	0.999647	0.999770
8th-order	strain	0.268261	0.003586	0.000042	0.000003	0.000002
	surface	0.998396	1.004074	1.001673	1.000419	1.000031
	potential	1.266657	1.007659	1.001715	1.000421	1.000033

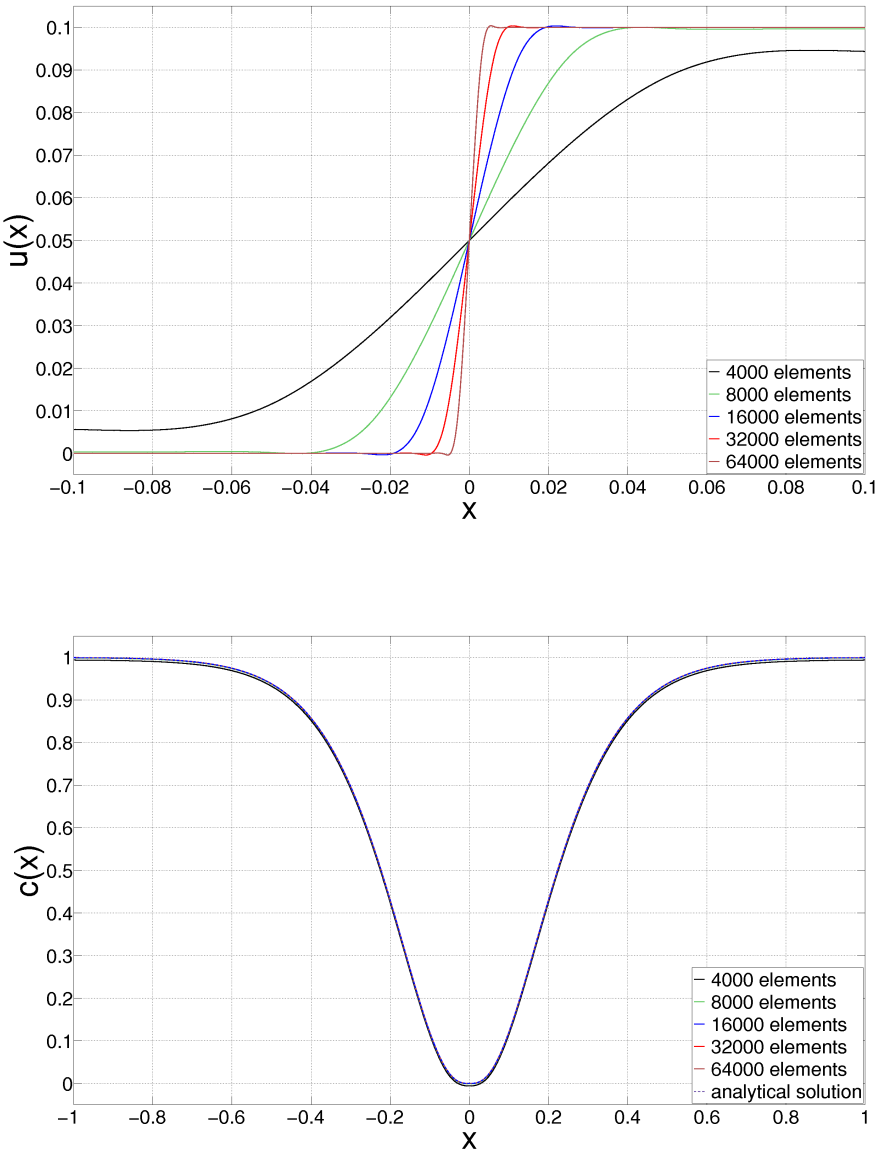

FIGURE 5.1. The displacement and phase fields from the sixth-order theory.

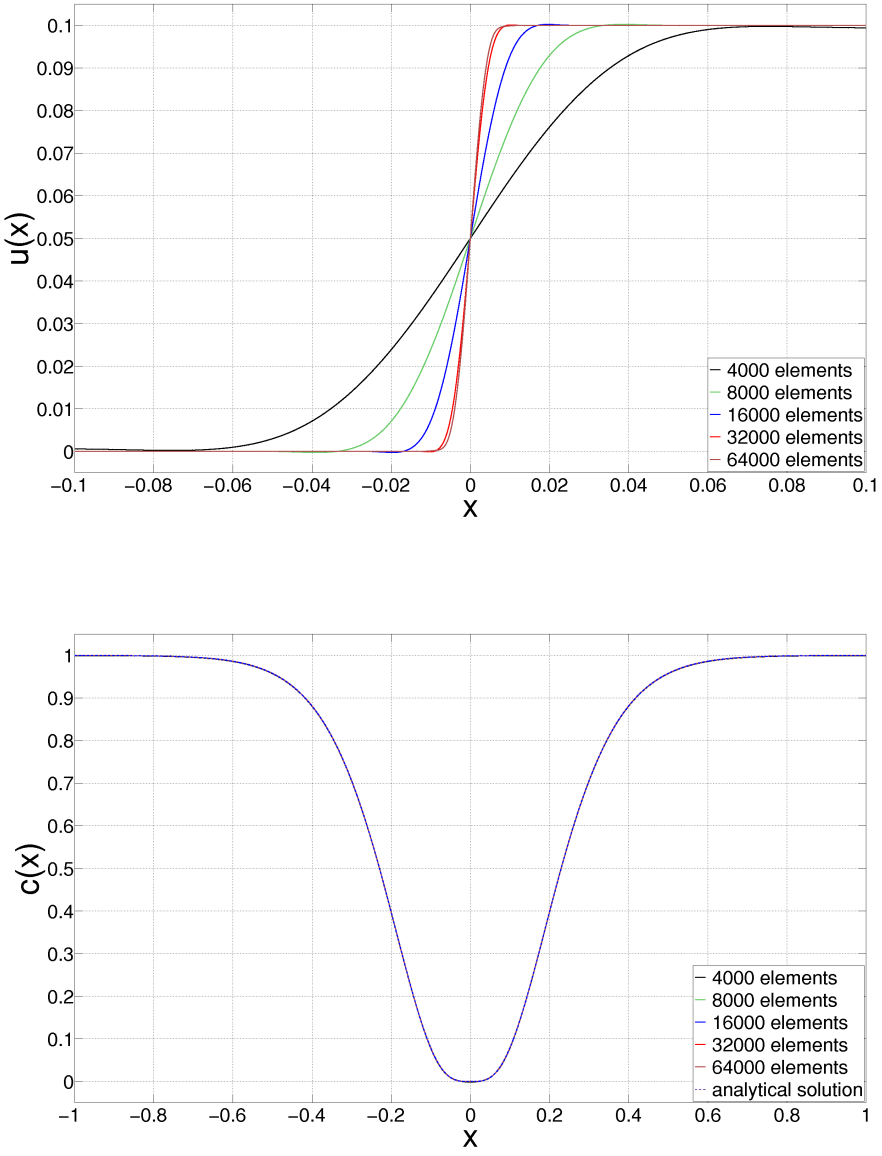

FIGURE 5.2. The displacement and phase fields from the eighth-order theory.

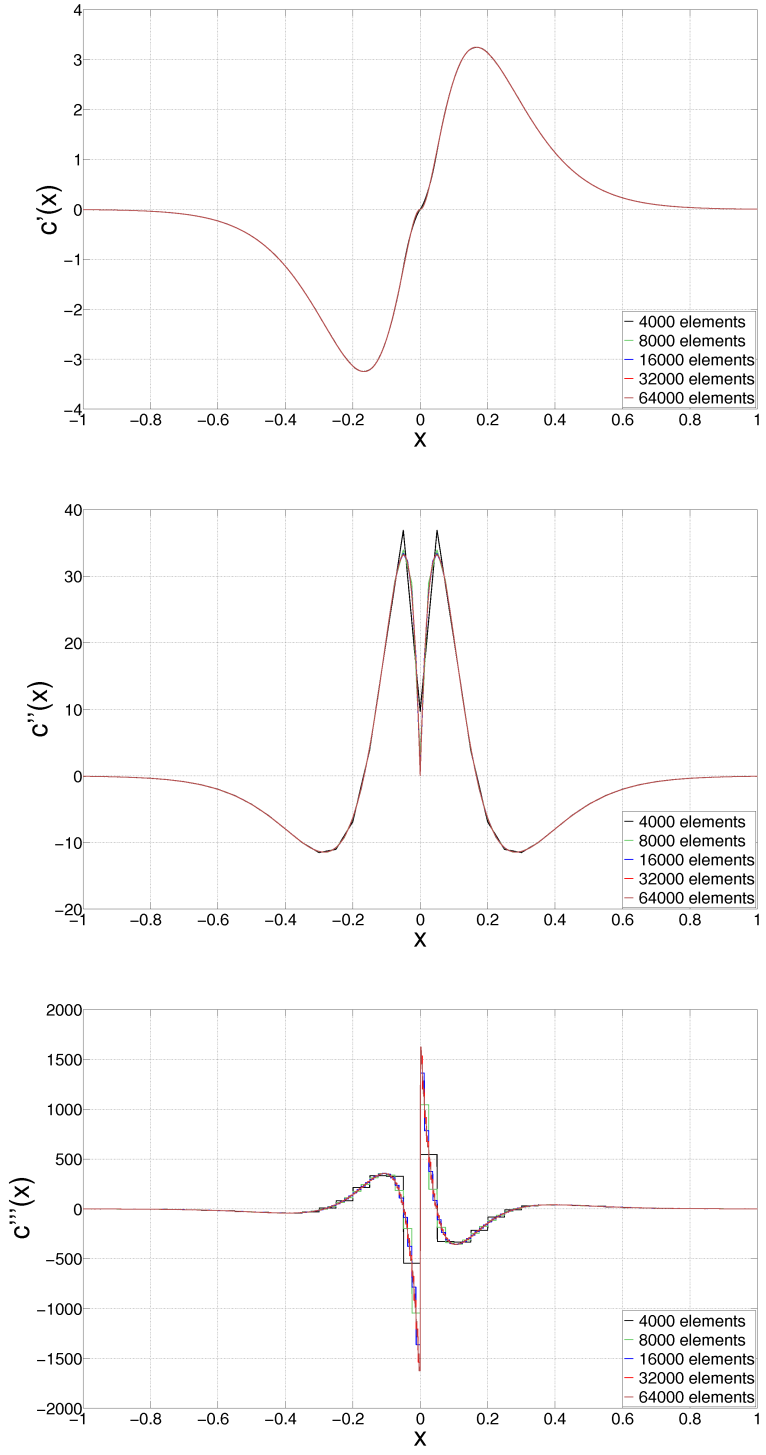

FIGURE 5.3. Derivatives of the phase field for the sixth-order theory. We get $c_h'(0), c_h''(0) \to 0$, as predicted by theory. Of course, $c_h'''(0) \neq 0$.

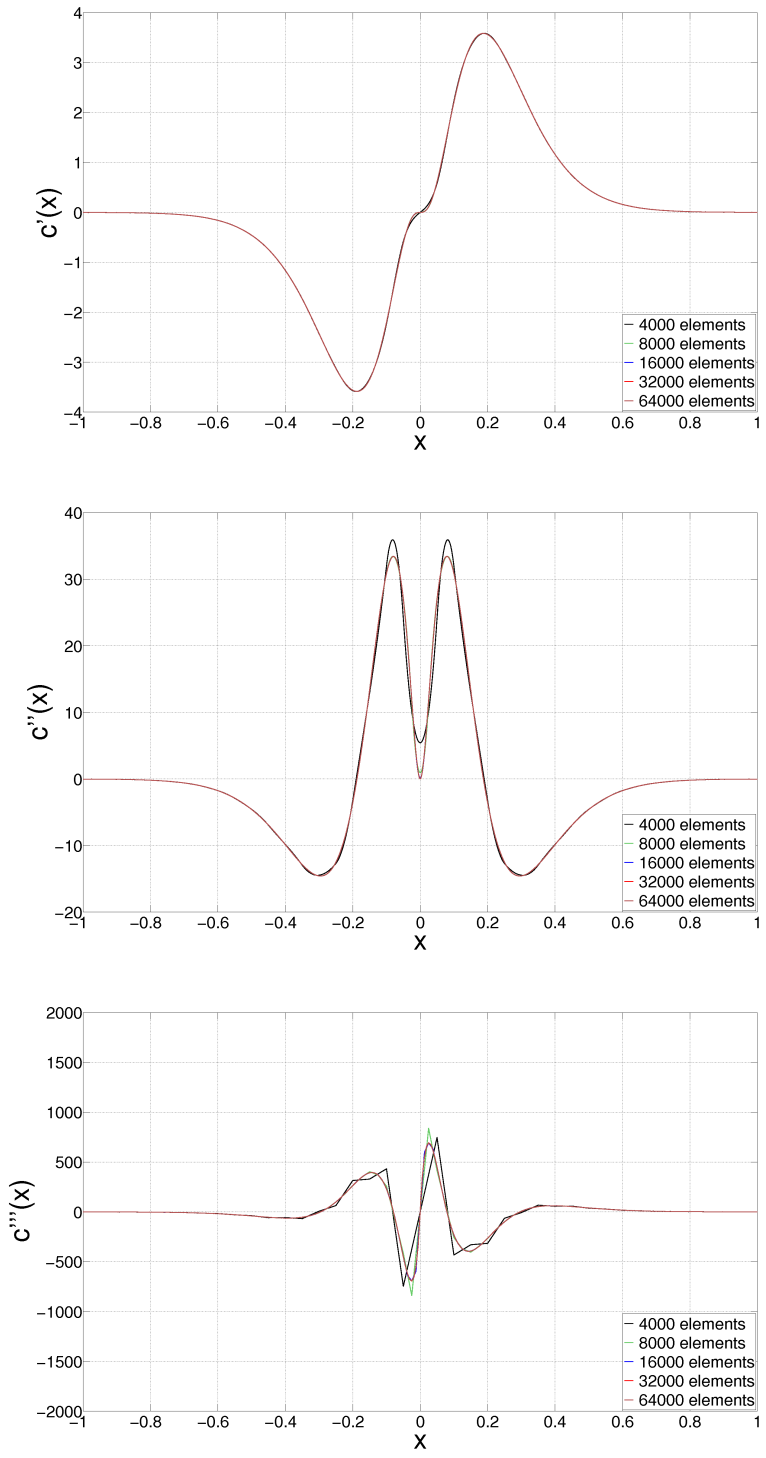

FIGURE 5.4. Derivatives of the phase field for the eighth-order theory. Again, we get $c_h'(0)$, $c_h''(0)$, $c_h'''(0) \to 0$, as predicted by theory.

It is clear from the table that, when we use the 6th- and 8th-order theories, the strain, surface, and potential energies converge to the right values at a faster rate. Figures 5.5 and 5.6 show the log-log plot of the errors versus the mesh size (these include the results for 128000 elements, which are not included in the table):

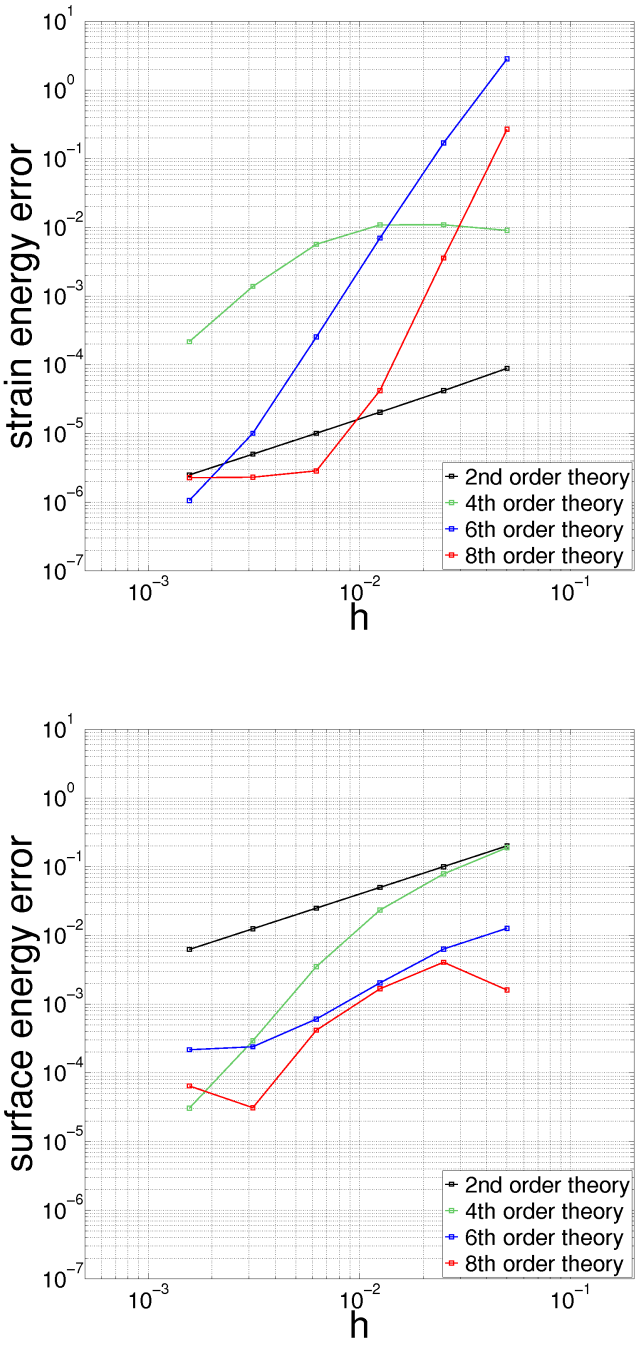

FIGURE 5.5. The strain energy and surface energy errors are plotted against the mesh size.

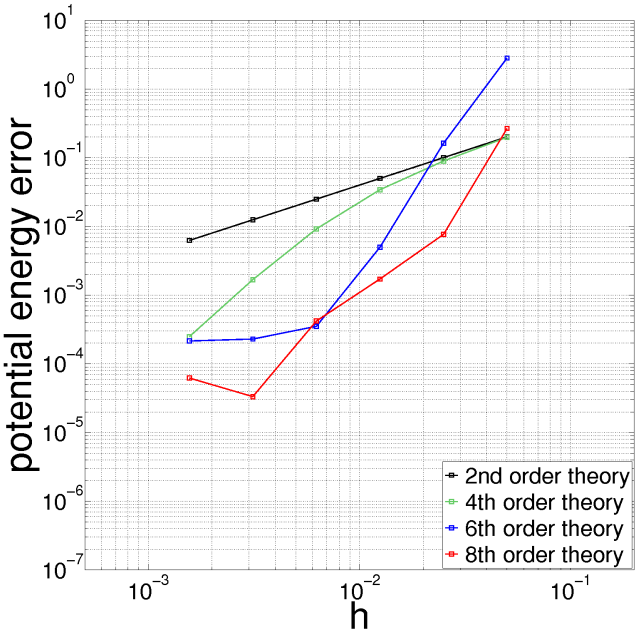

FIGURE 5.6. The potential energy error is plotted against the mesh size.

Unfortunately, we see a stagnation in convergence for the 6th- and 8th-order theories when the mesh is highly refined (for 64000 and 128000 elements). Figure 5.2 shows that the displacement field for the 8th-order theory stops getting sharper at 64000 elements. This is surprising because, if the FE solution of the phase field is accurate, then we know from our analysis of the decoupled problem in Section 3.1 that the displacement field will get sharper as $h \to 0$. It is not clear if the stagnation resulted from round-off errors in calculations, or indicates that the parameter k, which had been kept constant as 10^6, needs to depend on the mesh size h. The eigenvalue analysis that was mentioned before may clarify this.

For the moment, we write down the rates of convergence for the best case scenario: For each energy, we find the least-squares line over three consecutive mesh sizes, starting at 8000 elements. We take the maximum of the three slopes for the rate of convergence.

theory	rate of convergence		
	strain	surface	potential
2nd-order	1.028	1.002	1.002
4th-order	2.355	3.425	2.608
6th-order	4.721	1.690	4.424
8th-order	5.144	2.874	2.841